Brazil Nut Effect Drives Pattern Formation in Early Mammalian Embryos

Zheng Guo[1,#], Jie Yao[1,#], Xu Zheng[2,#], Jialing Cao[1], Shuyu Guo[1], Dandan Qin[3], Zheng Gao[5], Min Tan[1], Bo Wang[6], Fanzhe Meng[1], Jing Zhang[4], Zai Chang[4], Lei Li[3], Jing Du[1 *], and Yubo Fan[1*]

[1] Key Laboratory for Biomechanics and Mechanobiology of Ministry of Education, Beijing Advanced Innovation Centre for Biomedical Engineering, School of Biological Science and Medical Engineering, Beihang University, Beijing 100191, China

[2] State Key Laboratory of Nonlinear Mechanics, Beijing Key Laboratory of Engineered Construction and Mechanobiology, Institute of Mechanics, Chinese Academy of Sciences, Beijing 100190, China

[3] State Key Laboratory of Stem Cell and Reproductive Biology, Institute of Zoology, Chinese Academy of Sciences, Beijing 100101, China

[4] Laboratory Animal Research Center, Tsinghua University, Beijing 100084, China

[5] Center for Reproductive Medicine,Key laboratory for Major Obstetric Diseases of Guangdong Province,The Third Affiliated Hospital of Guangzhou Medical University,Guangzhou 510150, China

[6] Northwest Institute of Plateau Biology, Chinese Academy of Sciences, Xining 810008, China

[*] Correspondence: dujing@buaa.edu.cn (J.D.) and yubofan@buaa.edu.cn (Y.F.)

ABSTRACT

Since early mammalian embryos lack chemical gradients, the pattern formation mechanism is an open question. During the second cell fate decision of mouse embryos, the inner cell mass (ICM) segregates into topographically regionalized epiblast (EPI) and primitive endoderm (PrE) layers. Here, we report that the cell segregation process coincides with an emerged periodic expansion-contraction vibration of the blastocyst cavity, which induces a phase transition in the ICM compartment to a higher fluidity state. By experiments and modeling, we demonstrate that the spatial segregation of PrE and EPI precursors is mediated by a “Brazil nut effect”-like viscous segregation mechanism in which the vibration of the cavity induces cyclic directional tissue flows in the compartment of the ICM, which drives the separation and asymmetric migration of PrE and EPI precursors through granular segregation biased by different levels of particle adhesivity and sizes. Furthermore, cyclic embryo vibration also regulates the gene expression of PrE and EPI precursors through mechanotransduction by YAP. Our findings unveil a fundamental mechanism for ensuring the robustness of cell segregation and pattern formation, which is driven by the global geometry and mechanical behavior of early embryos.

KEY WORDS: vibration, viscous segregation, Brazil nut effect, pattern formation, PrE/EPI segregation, cell fate specification

INTRODUCTION

Spatiotemporally accurate pattern formation is very common in embryonic development. However, in early mammalian embryos, which consist of few types of cells, there is a lack of chemical gradients for pattern formation. In early mouse embryos, the first cell lineage specification begins at the 8- to 16-cell stage, resulting in extraembryonic trophectoderm (TE) formation by polar cells enclosing the pluripotent inner cell mass (ICM) composed of apolar cells [1]. At approximately the 32-cell stage, blastocysts are formed as a hyperosmotic fluid-filled cavity that appears at the interface of the ICM and TE by NA+/K+ ATPases in TE cells [2-4]. After the second cell fate decision, ICM cells are further segregated into two topographically regionalized lineages, the epiblast (EPI) and primitive endoderm (PrE). EPI is the precursor cell lineage of the future fetus [5,6], while PrE is a morphologically distinct epithelium separating the epiblast from the blastocyst cavity and is important for the establishment of the yolk sac [7-9]. Thus, at the time of implantation, the embryo is patterned as a pluripotent epiblast localized beside a fluid lumen and encapsulated by two extraembryonic tissues—the TE and the PrE.

At present, the factors that are considered necessary for the plasticity of mammalian embryonic development include geometric constraints, feedback between mechanical and biochemical factors, and cellular heterogeneity[10].Progenitors of EPI/PrE lineages can be first identified in early blastocysts by the expression of Nanog in EPI precursors and Gata6 in PrE precursors [11]. Initially, in the early stages of blastocyst development, EPI precursor cells and PrE precursor cells exist in a mixed "salt and pepper"-like distribution throughout the ICM compartment [12,13]. During blastocyst development, EPI and PrE cells are segregated by cell polarity (positional effect) and downregulation of the PrE transcriptional program in internal ICM cells [11-13]. The FGF/ERK signaling pathway has been shown to bias the EPI/PrE fate choice during blastocyst development. EPI precursor cells express FGF4 ligands, while PrE precursor cells upregulate FGF receptor 2 (FGFR2) expression [14,15]. FGF4 in ICM cells is elevated by Oct4 and Sox2 and binds to FGFR2 in adjacent cells to downregulate Nanog expression and upregulate Gata6 expression [16-18]. The whole process is accompanied by cell migration in the ICM, indicating a cell sorting process. Differential adhesion-mediated cell sorting processes have been theoretically proposed for the segregation of ICM cells. However, it has not been confirmed in vivo and guarantees only the separation of

EPI/PrE precursor cells. The directional signal that drives PrE and EPI precursor cells to allocate to their target positions to complete two-layer pattern formation has remained an open question for a long time.

In this work, combining experiments and modeling, we demonstrate that the spatial segregation and allocation of PrE and EPI precursors is mediated by a “Brazil nut effect”-like viscous segregation mechanism.

RESULTS

1. Topographical regionalization of PrE/EPI layers requires blastocoel vibration

It has been reported that during the development of blastocysts, PrE precursors move toward the ICM-cavity interface, whereas EPI cells retain inside the ICM compartment [19]. In our experiment, we visualized the migration of PrE precursors from stage E3.5 through time-lapse imaging of PrE-specific single-cell resolution reporter (*Pdgfra*$^{H2B\text{-}GFP/+}$, [20]) embryos (Figure 1a, b and Supplemental movie S1). By analyzing the relative distance of the GFP-positive cells to the center of the ICM surface [19] (Figure 1c), we found that at the beginning, no significant migration of PrE precursors was observed, and after 8.5 hr (approximately stage E3.75), the distance of GFP-positive cells to the ICM surface was progressively reduced, indicating that the relative allocation of PrE precursors tended to approach the center of the ICM surface after E3.75 (Figure 1d and e). Concurrently, we found that at the beginning of observation, the cavity of the blastocyst continuously expanded, and after E3.75, the blastocoel began to display rhythmic vibration (Figure 1f, g and Supplemental movie S2), which was accompanied by the significant migration of PrE precursors (Figure 1d and e). Interestingly, during rhythmic embryo vibration, each cavity contraction was always coincident with a prominent migration of PrE cells toward the ICM surface (Figure 1e and g). Moreover, accompanied with the emergence of rhythmic embryo vibration, the collective cellular motion in ICM compartment was switched from relatively static state to dynamic state, indicated by particle imaging velocity (PIV) analysis (Figure 1 h, i and Supplemental movie S3). This fluidity transition of ICM was also indicated by assessing the cell shape index p^0, the median ratio of the perimeter to the square root area of the cells. According to the vertex model, if the cell shape index of the system increases to $p^{*0} \approx 3.81$, a transition from a jammed, solid-like state to an unjammed, fluid-like state occurs [21]. The cell shape index in blastocysts after E3.75 was significant higher than early blastocysts which were prior to the emergence of rhythmic embryo vibration (Supplementary Figure S1). These observations indicate a possible correlation between PrE cell movement and blastocoel vibration.

The formation and expansion of the blastocyst cavity stems from the hyperosmotic fluid in the cavity, which generates pressure on the outside TE layer. As the TE layer bears significant tension,

when its integrity is disrupted by cell division, rapid cavity contraction occurs [22,23]. By assessing the tension of embryos indicated by the deformation of TE cells (Supplemental Figure S2a-c) and cavity recoil speed after UV laser cutting (Supplemental Figure S2d and e), we showed that cortical tension first increased and then declined during blastocyst development. Thus, we segmented the course of blastocyst development from E3.5 to E4.25 into 4 phases according to cortical tension and found that the vibration frequency of the embryo was increased at phases III and IV (Supplemental Figure S2f). Meanwhile, significant movement of PrE precursors to the cavity surface occurred at phases III and IV, when the embryo showed drastic vibration (Supplemental Figure S2g). The embryo vibration and migration of PrE precursors showed a positive correlation with each other during blastocyst development (Supplemental Figure S2h).

Next, to assess whether the cyclic vibration of blastocysts is essential for the directed movement of PrE cells to ICM surface, we suppressed embryo vibration by decreasing hydraulic pressure with hyperosmotic culture medium. The results showed that compared with the control group (cultured in normal KSOM medium), the cell tension and frequency of blastocyst vibration were both significantly reduced in the hyperosmotic treatment group (Figure 2a and b), and cell motility was significantly inhibited by hypertonic treatment (Figure 2c, d and Supplemental movie S4). As mentioned above, contraction of the blastocyst cavity was generated by cell division in the TE layer to release cortical tension. Embryos were treated with Anphidicolin to prevent cell division. As shown in Figure 2e, cavity contraction was reduced by inhibition of cell division. Moreover, ICM fluidity and PrE precursors movement were both significantly suppressed by Anphidicolin-treatment (Figure 2f-i). To further evaluate the function of cyclic vibration in the spatial segregation of PrE/EPI cells, *Pdgfra*$^{H2B\text{-}GFP/+}$ embryos were treated with hypertonic medium or normal medium from stage E3.5 (Figure 2j). At the end of 21 hr of treatment, GFP-positive cells were enriched at the ICM/cavity boundary in the control embryos, while the distribution of GFP-positive cells was still random in the hypertonic group (Figure 2k and l). Then, the embryos in hypertonic medium were washed out and moved to KSOM medium for continuous culture (Figure 2j). After 24 hr, GFP-positive cells were layered at the boundary of the ICM and blastocyst cavity in both groups (Figure 2k and l), indicating that interruption of cavity vibration prevented the segregation of PrE/EPI. These results suggest that the cyclic vibration of blastocysts

is essential for the topographical regionalization of PrE/EPI layers.

2. Embryo vibration induces PrE/EPI pattern formation through viscous segregation

Next, we sought to determine the mechanism underlying the promotion of PrE/EPI segregation by embryonic vibration. As mentioned above, embryo vibration elevated the fluidity of ICM compartment (Figure 1h, i and Figure 2h, i). Further study showed that during a period of contraction-expansion vibration, a converged tissue flow from the TE side toward the center of the ICM/cavity boundary was observed in the ICM compartment after each contraction. Moreover, the direction of the tissue flow was coincident with the movement of PrE cells (Figure 3b and Supplemental movie S5). Meanwhile, during the expansion of blastocoels, significant tissue flow was observed at the ICM surface parallel to the ICM/cavity boundary, which was accompanied by the lateral movement of PrE cells (Figure 3c, d and Supplemental movie S6). By mechanical analysis and simulation, we demonstrated that the dynamic tissue flow stemmed from the contraction or expansion of the embryo (Figure 3e, Supplemental movie S7, and Mechanical Model in the Supplemental materials). Since the time scale of the contraction phase was much shorter than that of the expansion phase, through several repetitions of the slow-expansion/rapid-contraction period, ratchet effect would be introduced which led to symmetry-breaking and direct cell migration [24]. On the other hand, numeric evidence have shown that during the segregation of EPI and PrE precursors, these two types of cells showed differences in cohesive property and motility. Compared with EPI precursors, PrE precursors possess lower cohesiveness and higher mobility [25-31]. We also found that, during blastocyst development, an increased cell aggregation tendency was observed in EPI cells compared with PrE cells (Figure 3f). Due to the unequal interval and transport ability between slow expansion and rapid contraction, the PrE cells with low cohesiveness and high mobility can be transported towards the center of the blastocyst. This mechanism is analogous to the viscous segregation of mixed granules based on different adhesive properties under exogenous energy input, for example, the “Brazil nut effect”. The Brazilian nut effect means that if a pile of nuts of different sizes is mixed into a container and then an additional vibration is applied, the largest Brazilian nut will usually rise to the surface,

while the smaller other nuts will settle to the bottom, which has important implications for many industrial processes and geophysical processes[32-35]. In our system, the vibration of the embryo provides an exogenous energy input as disturbance and caused phase transition with increased cell convection in the ICM compartment, which gave rise to the segregation of PrE and EPI cells depending on their distinct cohesiveness and cell cluster size. This hypothesis could be supported by a transient intermediate state which was observed during PrE/EPI segregation before pattern formation completion, in which Pdgfrα-positive cells were enriched as an "inverted pyramid" at the central region of the ICM/cavity boundary and embraced by Nanog-positive cells (Figure 3g and h).

To evaluate this Brazil nut effect hypothesis, we monitored the migration of chemically inert fluorescent microbeads that were injected into the ICM compartment of early blastocysts (Figure 4a). The results showed that although the microbeads were initially randomly distributed in the ICM compartment, they were enriched at the interface of the ICM/cavity in most embryos after several hours (Figure 4b and c). Directed movement of microbeads was also observed after embryo contraction (Figure 4d and Supplemental movie S8). Next, we conducted computational modeling using a finite element simulation and found that the allocation and sorting of PrE/EPI precursors during the slow-expansion/rapid-contraction periods could be recapitulated by the segregation of cohesive granular flow driven by asymmetry vibration (Figure 4e, Supplemental Figure S3a, Supplemental movie S9 and Mechanical model in the Supplemental materials). Moreover, the simulation results predicted that successful segregation of cells relies on the difference in cell cohesive properties and the asymmetry of expansion-contraction speed (Figure 4e).

On the other hand, when the embryo was in the "inverted pyramid" intermediate state, position effect (e.g. polarity signals) together with the lateral tissue flow at the surface of the ICM during the expansion of the blastocyst cavity could drive the rearrangement of Pdgfrα-positive cells to line as a monolayer. In addition, we found significant F-actin bundles were enriched at the boundary of Pdgfrα-positive cells and the cavity in the "inverted pyramid" intermediate state

(Supplemental Figure S3b), and the outermost Pdgfrα-positive cells displayed a "Rose-like" distribution at the surface of the ICM (Supplemental Figure S3c), indicating the contribution of actomyosin contractility in the epithelialization of PrE cells to complete the pattern formation of ICM. Taken together, we propose a model for the topographical regionalization of the ICM during blastocyst development in which the asymmetric tissue flow inside the ICM compartment generated by the cyclic contraction-expansion of the embryo induces PrE precursors moving toward the center of the ICM/cavity boundary to form an "inverted pyramid" through viscous segregation. Then, the lateral tissue flow at the surface of the ICM during the expansion phase together with chemical signal drives PrE cells to rearrange as a monolayer epithelium to form a two-layer pattern. This "Brazil nut effect" model of ICM segregation is illustrated in Figure 4f.

3. PrE/EPI spatial segregation and lineage specification could be controlled by embryo vibration

To further investigate the function of embryo vibration in the lineage specification of PrE/EPI, we interrupted blastocoel tension by different chemical and physical treatments. As mentioned above, hypertonicity treatment reduced TE tension (Figure 2a) and suppressed embryo vibration (Figure 2b) as well as the migration of Pdgfrα-positive cells (Figure 2c, d and j-l). We further confirmed that hypertonic treatment of embryos from stage E3.5 for 24 hrs significantly suppressed the spatial segregation of PrE/EPI precursors compared with control embryos (Figure 5a and b). Moreover, the lineage specification of PrE/EPI cells was also interrupted by hypotonic treatment (Figure 5a and c-e). Since the hyperosmotic solution secreted into the blastocyst cavity is mediated by the Na^+/H^+ exchanger isoform NHE-3 in TE cells, we treated embryos with the NHE3 inhibitor S3226, which has been shown to inhibit the expansion of blastocysts [36]. The vibration frequency of the blastocyst cavity in the S3226 group was significantly reduced compared with that of the control group (Supplemental Figure S4a). The results showed that the spatial segregation and lineage specification were both inhibited by S3226 treatment (Supplemental Figure S4b-f). It has been demonstrated that the expansion and contraction of the blastocyst cavity requires cell contractility by the actomyosin cytoskeleton [23]. Thus, we treated

embryos with the actomyosin inhibitors blebbistatin (Bleb) and cytochalasin A (CA) to inhibit embryo vibration (Supplemental Figure S5a and S6a). Both of these actomyosin inhibitor treatments dramatically disrupted the spatial segregation of PrE/EPI cells and prevented their lineage specification (Supplemental Figure S5 and S6). Together, these data show that interruption of embryo vibration inhibits PrE/EPI spatial segregation and lineage specification.

Next, we wondered whether the segregation of PrE/EPI cells could be facilitated by reinforced embryo vibration. We first treated E3.25 stage embryos with hypotonic medium, which significantly increased the frequency of embryo vibration (Figure 6a). At the end of treatment for 24 hrs, the spatial segregation and lineage specification of EPI/PrE cells were almost complete in the hypotonic group, while these two types of cells were still mixed in the control embryos (Figure 6b-f). This phenomenon was confirmed by lysophosphatidic acid (LPA) treatment, which could promote the activity of NHE-3 [37]. The treatment of LPA also enhanced embryo vibrations (Supplemental Figure S7a) and accelerated the spatial segregation and lineage specification of PrE/EPI cells EPI/PrE segregation (Supplemental Figure S7b-f). In summary, these results indicate that embryo vibration plays a pivotal role in the spatial segregation and fate decision of PrE/EPI.

4. PrE/EPI spatial segregation and lineage specification maintenance requires embryo vibration during the initial stage after two-layer pattern formation

We noticed that the embryo vibration frequency remained at a high level at late blastocyst after pattern formation of PrE/EPI layers (phase IV in Supplemental Figure S2f). To determine whether the maintenance of ICM regionalization also requires vibration of the embryo, we monitored the effect of hypertonic treatment on the cell allocation dynamics in *Pdgfra*$^{H2B\text{-}GFP/+}$ blastocysts at different stages. We found that the segregation of PrE/EPI cells could be reversed when hypertonicity was applied at the initial stage after PrE/EPI (within ~3 hr after the “inverted pyramid” intermediate stage). However, when hypertonicity was treated to embryos several hours (at least ~5 hr) post the intermediate stage, the two-layer pattern could not be reversed (Figure 7a and b), indicating that the vibration of the embryo is required for the maintenance of the PrE/EPI regionalization at the initial stage after segregation.

To further determine the reversibility of lineage specification of PrE/EPI by vibration inhibition, WT embryos at E4.0 were collected; some were fixed as a control group, and others were treated with the NHE-3 inhibitor S3226 for 24 hrs (Figure 7c). While most of the control embryos had completed PrE/EPI spatial segregation, most of S3226-treated embryos showed a mixed distribution of cells expressing Nanog or Pdgfrα (Figure 7d and e). Moreover, the lineage specification of PrE/EPI was also interrupted by S3226-treatment (Figure 7f-h). Similar results were observed in embryos treated with hypertonic medium (Supplemental Figure S8). These results suggest that during the initial stage after PrE/EPI two-layer pattern formation, the spatial segregation and lineage specification are both sustained partially by embryo vibration.

5. Embryo vibration regulates the gene expression of PrE and EPI precursors through mechanotransduction by YAP

To determine the mechanism underlying the promotion effect of embryo vibration in PrE/EPI lineage specification, we analyzed the gene expression level during segregation process. We found that in *Pdgfra*$^{H2B\text{-}GFP/+}$ embryos, the GFP expression intensity was progressively enhanced after the beginning of embryo vibration (8.5 hr) during the migration of Pdgfrα-positive cells (Figure 8a–c and in the Supplemental movie S10), indicating a positive correlation of gene expression of PrE marker gene and embryo vibration. Moreover, the expression level of Pdgfrα was significantly reduced by hypertonic treatment (Figure 8d) and increased by hypotonic medium (Figure 8e), whereas Nanog expression was little affected by these treatments. Moreover, the ratio of Nanog-positive to Pdgfrα-positive cells was also significantly induced by hypertonicity and reduced by hypotonicity (Figure 8f). Similar results were observed in embryos treated with NHE-3 inhibitor, LPA, blebbistatin, and CA (Supplemental Figure S9). These results indicate that embryo vibration contributes to the gene expression of PrE/EPI precursors during spatial segregation.

In the first lineage specification of mouse embryo, the formation of ICM/TE pattern due to the asymmetric activation of Yes-associated protein (YAP), which has been demonstrated to be a conserved mechanical sensor and is involved in diverse developmental processes [38]. There is

evidence that YAP signaling increases the expression of FGF receptors (FGFRs) in embryonic neural stem cells and lung cancer samples [39,40]. Thus, we assessed the potential role of YAP in the lineage specification of PrE/EPI promoted by embryo vibration. During the development of blastocysts, the levels of nuclear YAP in PrE and EPI precursors were comparable at phase I, however, significant difference in the nuclear YAP level in PrE and EPI precursors was observed after phase II (Figure 8g and h). Moreover, the nuclear/cytoplasmic ratio of YAP showed an increasing tendency in PrE precursors, while this ratio was gradually reduced in EPI cells (Figure 8g and h). Interruption of blastocoel vibration by CA treatment significantly suppressed the nuclear level of YAP, while promoted vibration by hypotonic medium elevated the nuclear level of YAP (Figure 8i and j). Since the lineage specification of PrE/EPI is completed at late phase III, these observations indicate a possible role of YAP in the regulation of PrE/EPI cell fate by embryo vibration. To evaluate this hypothesis, YAP activity was reduced by its inhibitor Verteporfin (VP) during the development of blastocyst. As shown in Figure 9, VP treatment significantly disrupted the spatial segregation and lineage segregation of PrE/EPI layers. These results indicate that embryo vibration regulates gene expression mainly through mechanosensing by YAP during the spatial segregation of PrE/EPI layers.

DISCUSSION

In the salt and pepper model, the random expression of the FGF4 gene in ICM cells affects the gene expression of neighboring cells [11,41,42]. PrE cells finally gather near the blastocyst cavity under the action of positional induction [43]. Positional induction in the existing model explains only why the PrE cell determines its final position through the cell sorting process [12], and the mechanism of how PrE and EPI cells allocate to their target position is unclear [44]. Tissue flow is common in the process of embryo development and organ formation and is often accompanied by the process of cell migration and cell sorting [45]. In our model, the tissue flow of the ICM caused by TE tension shows a direction converging toward the surface of the ICM during the rapid contraction phase. The sensitivity of cells to the tissue flow is dependent on its adhesive properties. In the process of blastocyst rhythmic vibration, EPI cells with strong adhesiveness are more likely to gather together, and PrE cells with weak adhesiveness are more likely to fill the gaps between EPI cells. This different adhesion-dependent cell regionalization is also observed during the development of zebrafish embryos [46].

In the development of many animal embryos, morphogens are involved in cell fate determination. For example, the fate of the zebrafish mesoderm is regulated by morphogens [47]. In the development of the spinal cord of zebrafish, morphogens work together with cells with different adhesion to enable cells to construct the body accurately and consistently [46]. In early mouse embryos, there is no morphogen gradient has been reported for cell sorting. There are few mechanisms that can replace morphogens to drive the regionalization of cell spatial distribution. In Dictyostelium without morphogens, patterns are formed through the nonmorphogenetic mechanism of scattered differentiation and sorting out [48]. This mechanism without morphogens believes that the whole process consists of two parts: different cells are formed from the precursor pool under conditions independent of location; cells are sorted by physical movement. Although this mechanism escapes the limitations of morphogens, there is no in-depth study on how cells

move physically and the source of driving force. A computational model of cell sorting indicated that the asymmetric affinity between EPI and PrE cells is not enough to complete spatial isolation in mouse embryos [28,29]. Our results show that in addition to the differential adhesion between EPI and PrE cells, energy input mediated by the mechanical vibration of the cavity is required to complete the segregation of the spatial location. It is generally accompanied by the appearance of the cavity system in embryonic development and organogenesis. The appearance and expansion of the cavity system must be accompanied with the generation and accumulation of mechanical energy. When the energy of the cavity system has accumulated to a certain extent and reaches the threshold, it is released and converted in other forms, which affects the entire system. The function of cavity expansion in the lineage specification of PrE/EPI cells has also been observed in a recent study. In our results, we found that when embryo vibration was suppressed by cell division inhibition without affecting cavity expansion, the position of the PrE cell is relatively static (Figure 2e-g). Since the vibration depends on the tension generated by cavity expansion, these results indicate that cavity expansion is an essential requirement for embryo vibration and pattern formation. From this point of view, the cavity system is conservative and stable, with high universality. In this case, the accumulation of mechanical force in the blastocyst cavity is transformed and transmitted into the movement of differentially adhered cells in the ICM. The function of tissue-scale wave of mechanochemical propagation in embryonic development has also been observed in other species [49].

Our results are the first to propose that in early mammalian embryonic development without a specific morphogen, the mechanical force and energy mediated by the vibration of the cavity system are transferred to directional tissue flow which drives spatial segregation of PrE and EPI precursors by a “Brazil nut effect”-like viscous segregation mechanism. This cell sorting mode driven by the global geometry and mechanical behavior is very conservative and quite stable for ensuring the robustness of cell segregation and pattern formation in the development of embryos and organs. It is also helpful to guide the construction of artificial organizations for research or medical applications.

REFERENCES

1 Ziomek, C. A. & Johnson, M. H. Properties of polar and apolar cells from the 16-cell mouse morula. *Development Genes & Evolution* **190**, 287-296 (1981).

2 Watson, A. J. & Barcroft, L. C. Regulation of blastocyst formation. *Frontiers in Bioscience* **6**, D708-730 (2001).

3 Wiley, L. M. Cavitation in the mouse preimplantation embryo: Na/K-ATPase and the origin of nascent blastocoele fluid. *Developmental Biology* **105**, 330-342 (1984).

4 Violette, M. I., Madan, P. & Watson, A. J. Na+/K+-ATPase regulates tight junction formation and function during mouse preimplantation development. *Dev. Biol.* **289**, doi:10.1016/j.ydbio.2005.11.004 (2006).

5 Ian *et al.* Functional Expression Cloning of Nanog, a Pluripotency Sustaining Factor in Embryonic Stem Cells. *Cell* (2003).

6 Mitsui, K. *et al.* The homeoprotein Nanog is required for maintenance of pluripotency in mouse epiblast and ES cells. *Cell* **113**, 631-642 (2003).

7 Beddington, R. S. P. & Robertson, E. J. Anterior patterning in mouse. *Trends in Genetics* **14**, 277-283 (1998).

8 Janet Rossant, P. P. L. T. Emerging Asymmetry and Embryonic Patterning in Early Mouse Development. *Developmental Cell* **Volume 7, Issue 2**, Pages 155-164, doi:10.1016/j.devcel.2004.07.012. (2004).

9 Lu, C. C., Brennan, J. & Robertson, E. J. From fertilization to gastrulation: axis formation in the mouse embryo. *Current Opinion in Genetics & Development* **11**, 384-392 (2001).

10 Zhu, M. & Zernicka-Goetz, M. Principles of Self-Organization of the Mammalian Embryo. *Cell* **183** (2020).

11 Chazaud, C., Yamanaka, Y., Pawson, T. & Rossant, J. Early lineage segregation between epiblast and primitive endoderm in mouse blastocysts through the Grb2-MAPK pathway. *Developmental Cell* **10**, 615-624 (2006).

12 Meilhac, S. M. *et al.* Active cell movements coupled to positional induction are involved in lineage segregation in the mouse blastocyst. *Developmental Biology* **331**, 210-221 (2009).

13 Saiz, N., Grabarek, J. B., Sabherwal, N., Papalopulu, N. & Plusa, B. Atypical protein kinase C couples cell sorting with primitive endoderm maturation in the mouse blastocyst. *Development* **140**, 4311-4322 (2013).

14 Guo, G. *et al.* Resolution of Cell Fate Decisions Revealed by Single-Cell Gene Expression Analysis from Zygote to Blastocyst. *Developmental Cell* **18**, 675-685, doi:https://doi.org/10.1016/j.devcel.2010.02.012 (2010).

15 Ohnishi, Y. *et al.* Cell-to-cell expression variability followed by signal reinforcement progressively segregates early mouse lineages. *Nature Cell Biology* **16**, 27-37 (2014).

16 Frankenberg, S. *et al.* Primitive Endoderm Differentiates via a Three-Step Mechanism Involving Nanog and RTK Signaling. *Developmental Cell* **21**, 1005-1013, doi:https://doi.org/10.1016/j.devcel.2011.10.019 (2011).

17 Yamanaka, Y., Lanner, F. & Rossant, J. FGF signal-dependent segregation of primitive endoderm and epiblast in the mouse blastocyst. *Development* **137**, 715 (2010).

18 Artus, J., Kang, M., Cohen-Tannoudji, M. & Hadjantonakis, A. K. PDGF signaling is required for primitive endoderm cell survival in the inner cell mass of the mouse blastocyst. *Stem Cells* **31**, 1932-1941 (2013).

19 Ryan, A. Q., Chan, C. J., Graner, F. & Hiiragi, T. Lumen expansion facilitates epiblast-primitive endoderm fate specification in the mouse blastocyst formation. *bioRxiv*, 575282, doi:10.1101/575282 (2019).

20 Hamilton, T. G., Klinghoffer, R. A., Corrin, P. D. & Soriano, P. Evolutionary Divergence of Platelet-Derived Growth Factor Alpha Receptor Signaling Mechanisms. *Molecular & Cellular Biology* **23**, 4013 (2003).

21 Dapn, Opz, J. H., Schwarz, J. M. & Samannn, M. A density-independent rigidity transition in biological tissues. *Nature Physics* (2015).

22 Niimura, S. Time-lapse videomicrographic analyses of contractions in mouse blastocysts. *J. Reprod. Dev.* **49**, doi:10.1262/jrd.49.413 (2003).

23 Chan, C. J. *et al.* Hydraulic control of mammalian embryo size and cell fate. *Nature* **571**, 112-116 (2019).

24 Silva, C., De Vondel, J., Morelle, M. & Moshchalkov, V. Controlled multiple reversals of a ratchet effect. *Nature* **440**, 651-654 (2006).

25 Nissen, S. B., Perera, M., Gonzalez, J. M., Morgani, S. M. & Trusina, A. Four simple rules that are sufficient to generate the mammalian blastocyst. *Plos Biology* **15** (2017).

26 Canham, M., Sharov, A. A., Ko, M. S. H. & Brickman, J. Functional Heterogeneity of Embryonic Stem Cells Revealed through Translational Amplification of an Early Endodermal Transcript. *mechanisms of development* **8**, S280-S281 (2010).

27 Robson, P., Stein, P., Zhou, B., Schultz, R. M. & Baldwin, H. S. Inner Cell Mass-Specific Expression of a Cell Adhesion Molecule (PECAM-1/CD31) in the Mouse Blastocyst. *Developmental Biology* **234**, 317-329 (2001).

28 Krupinski, P., Chickarmane, V., Peterson, C. & Thieffry, D. Simulating the Mammalian Blastocyst - Molecular and Mechanical Interactions Pattern the Embryo. *PLOS Computational Biology* **7**, e1001128- (2011).

29 Yanagida, A. *et al.* Cell surface fluctuations regulate early embryonic lineage sorting. *bioRxiv*, 2020.2008.2016.250084, doi:10.1101/2020.08.16.250084 (2020).

30 Liebisch, T., Drusko, A., Mathew, B., Stelzer, E. H. K. & Matthus, F. Cell fate clusters in ICM organoids arise from cell fate heredity and division: a modelling approach. *Scientific Reports* **10** (2020).

31 Filimonow, K. *et al.* No evidence of involvement of E-cadherin in cell fate specification or the segregation of Epi and PrE in mouse blastocysts. *PLoS ONE* **14** (2019).

32 Johnson, C. G. *et al.* Grain-size segregation and levee formation in geophysical mass flows. *Journal of Geophysical Research Earth Surface* **117**, - (2013).

33 Li, Z. *et al.* Microscopic structure and dynamics study of granular segregation mechanism by cyclic shear. *Science Advances* **7**, eabe8737, doi:10.1126/sciadv.abe8737 (2021).

34 Umbanhowar, P. B., Lueptow, R. M. & Ottino, J. M. Modeling Segregation in Granular Flows. *Annual Review of Chemical and Biomolecular Engineering* **10** (2019).

35 Soko, M., Richardson, D. C., Patrick, M., Schwartz, S. R. & Ronald-Louis, B. The Brazil nut effect and its application to asteroids. *Monthly Notices of the Royal Astronomical Society*, 4 (2014).

36 Rikako *et al.* Na+/H+ Exchanger-3 is involved in mouse blastocyst formation. *Journal of Experimental Zoology Part A: Comparative Experimental Biology* (2004).

37 Lee-Kwon, W., Kawano, K., Choi, J. W., Kim, J. H. & Donowitz, M. Lysophosphatidic Acid Stimulates Brush Border Na+/H+ Exchanger 3 (NHE3) Activity by Increasing Its Exocytosis by an NHE3 Kinase A Regulatory Protein-dependent Mechanism. *Journal of Biological Chemistry* **278**, 16494-16501 (2003).

38 Nishioka, N. The Hippo signaling pathway components Lats and Yap pattern Tead4 activity to distinguish mouse trophectoderm from inner cell mass. *Dev. Cell* **16**, doi:10.1016/j.devcel.2009.02.003 (2009).

39 Dasol Han, S. M. L., Mookwang Kwon, Hogyun Noh, Ju Hyun Lee, Youngik Yoon, Jae Youl Cho, and Keejung Yoo. YAP Enhances FGF2-Dependent Neural Stem Cell Proliferation by Induction of FGF Receptor Expression. *Stem Cells and Development* **29**, 1240-1246, doi:10.1089/scd.2019.0281 (2020).

40 Lu, T. *et al.* The Hippo/YAP1 pathway interacts with FGFR1 signaling to maintain stemness in lung cancer. *Cancer Letters*, S0304383518301423 (2018).

41 Schrode, N., Saiz, N., Di?Talia, S. & Hadjantonakis, A. K. GATA6 levels modulate primitive endoderm cell fate choice and timing in the mouse blastocyst. *Developmental Cell* **29**, 454-467 (2014).

42 Kang, M., Garg, V. & Hadjantonakis, A. K. Lineage Establishment and Progression within the Inner Cell Mass of the Mouse Blastocyst Requires FGFR1 and FGFR2. *Developmental Cell*, S1534580717303854 (2017).

43 Piliszek, A. E., Plusa, B., Frankenberg, S., Artus, J. & Hadjantonakis, A.-K. Distinct sequential cell behaviours direct primitive endoderm formation in the mouse blastocyst. *Developmental Biology* (2008).

44 Xenopoulos, P., Kang, M., Puliafito, A., Ditalia, S. & Hadjantonakis, A. K. Heterogeneities in Nanog Expression Drive Stable Commitment to Pluripotency in the Mouse Blastocyst. *Cell Reports* **10**, 1508-1520 (2015).

45 Saadaoui, M., Rocancourt, D., Roussel, J., Corson, F. & Gros, J. J. S. A tensile ring drives tissue flows to shape the gastrulating amniote embryo. **367**, 453-458 (2020).

46 Tsai, T. Y.-C. *et al.* An adhesion code ensures robust pattern formation during tissue morphogenesis. *Science* **370**, 113-116, doi:10.1126/science.aba6637 (2020).

47 Barone *et al.* An Effective Feedback Loop between Cell-Cell Contact Duration and Morphogen Signaling Determines Cell Fate. *Developmental Cell* (2017).

48 Kay, R. R. & Thompson, C. R. L. Forming Patterns in Development without Morphogen Gradients: Scattered Differentiation and Sorting Out. *Cold Spring Harbor Perspectives in Biology* **1**, a001503 (2009).

49 Bailles, A. *et al.* Genetic induction and mechanochemical propagation of a morphogenetic wave. *Nature* (2019).

ACKNOWLEDGMENTS

This work was supported by the National Key R&D Program of China (2017YFA0506500,

2016YFC1102203, and 2016YFC1101100), the National Natural Science Foundation of China (31370018, 11972206, 11902114, 11421202, 11827803, and 11902020), and Fundamental Research Funds for the Central Universities (ZG140S1971).

AUTHOR CONTRIBUTIONS

Y.B.F. and J.D. designed the study and interpreted experiments. Z.G., J.C, and S.G. performed experiments. Y.J. and X.Z. did the mechanical modeling. D.D.Q., Z.G., L.L., J.Z., and Z.C. helped with the embryonic experiments. M.T., B.W., and F.Z.M helped with the statistical analysis of data. Y.B.F. and J.D. conceived and supervised this project and wrote the paper.

COMPETING INTERESTS

There are no competing interests

Figures

Figure 1

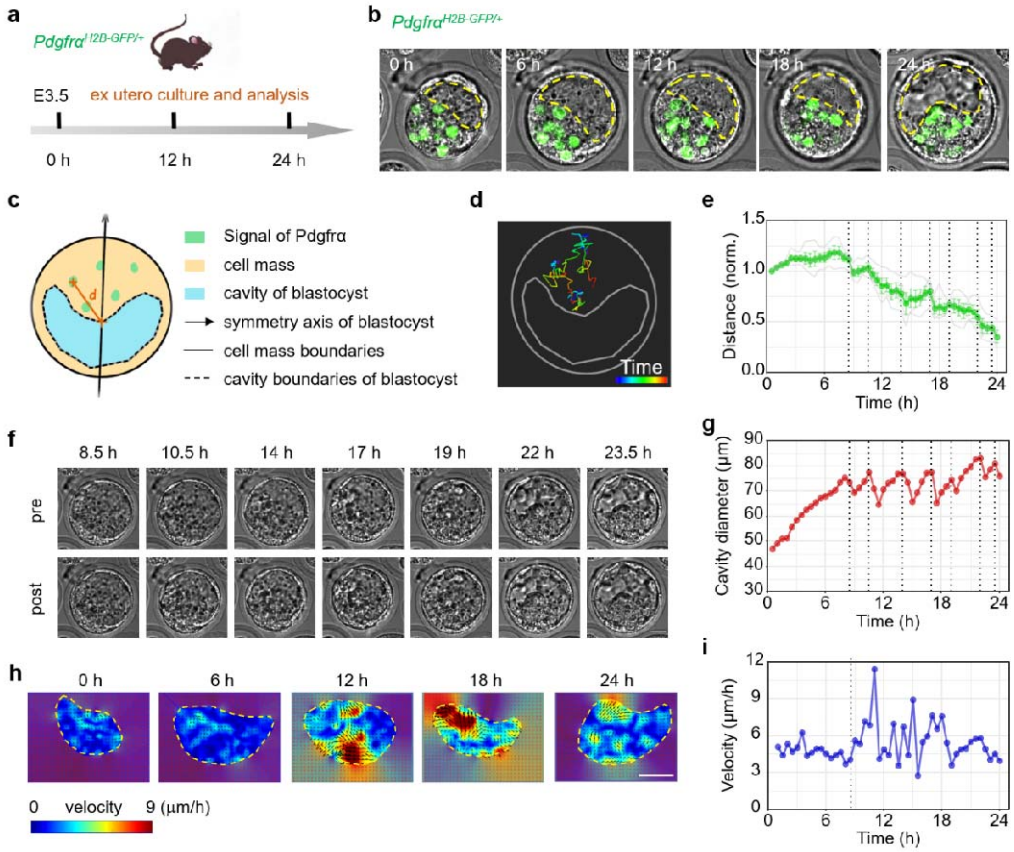

Figure 1.The migration of PrE precursors is consistent with the periodic vibration of the blastocyst (a) Schematic diagram of in vitro culture of *Pdgfrα*$^{H2B\text{-}GFP/+}$ mouse blastocysts. (b) Time-lapse image of a representative *Pdgfrα*$^{H2B\text{-}GFP/+}$ mouse blastocyst during development. The yellow dotted line denotes the boundary of the cavity. Time (Upper left) is shown as hour after E3.5. Scale bar, 20 μm. (c) Schematic diagram of measuring Pdgfrα-GFP positive cells to the center of the ICM surface. Connect the geometric center of the ICM with the geometric center of the cavity to obtain the symmetry axis of the embryo. The intersection of the symmetry axis of the embryo and the boundary of the ICM near the cavity is regarded as the center of ICM surface. Calculate the distance (d) from the center of the cell expressing *Pdgfrα*$^{H2B\text{-}GFP/+}$ to the center of ICM surface. (d) Trajectory of 4 Pdgfrα-GFP positive cells during blastocyst development. Time

bar (Lower right), 0 ~ 24 h. Scale bar, 20 μm. (e) Quantification of the distance of the Pdgfrα-GFP positive cells to the center of the ICM surface over time (thin gray lines are traces of individual cell, green line is traces of the average distance, dotted line indicates the moment when the blastocyst contracted, n = 4). (f) The representative images of blastocyst pre and post contraction in each period of vibration. Scale bar, 20 μm. (g) Quantification of the blastocyst diameter over time (dotted line indicates the moment when the blastocyst contracted). (h) Time-lapse of the heat map of the velocity magnitude filed in ICM during blastocyst development. The yellow dotted line denotes the boundary of ICM. Scale bar: 20 μm. (i) The statistical analysis of cell speed (rms velocity) measured by PIV in ICM compartment during blastocyst develpment. All of the results in (a) – (i) are obtained in the same representative embryo and repeated for at least three times.

Figure 2

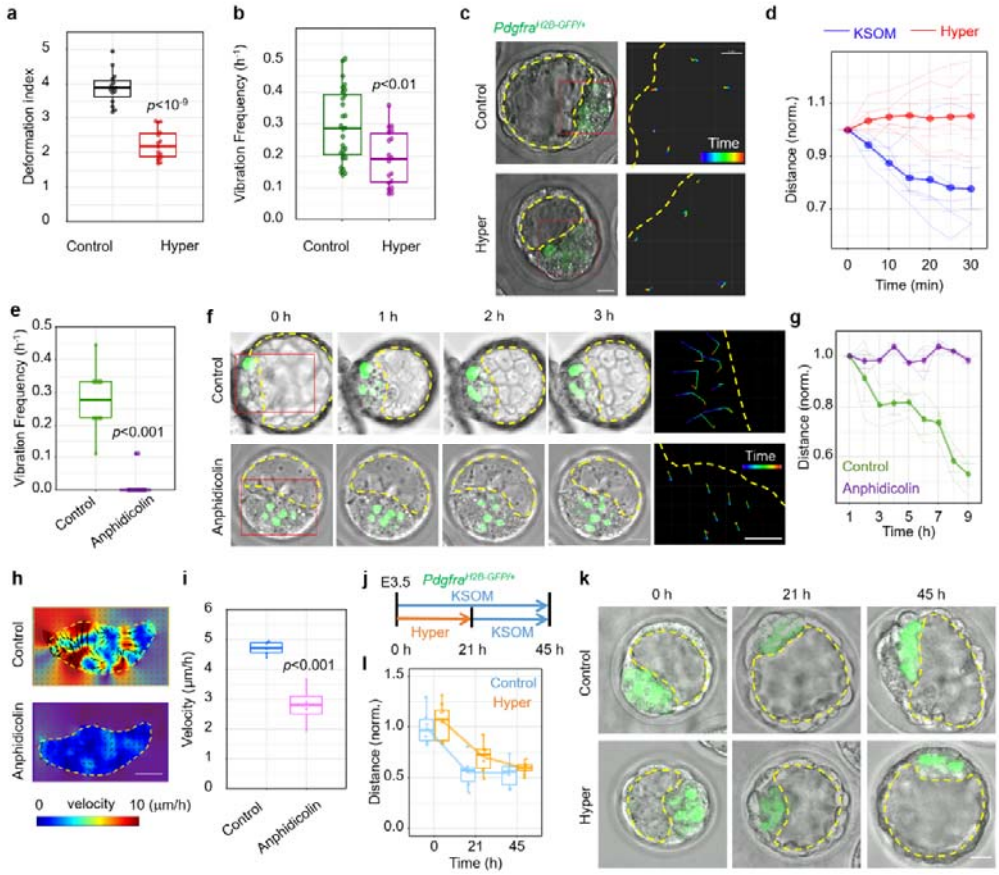

Figure 2. Inhibition of embryo vibration prevents the topographical regionalization of PrE (a) Deformation index of TE cells in control (n = 15 cells from 5 embryos) and hypertonic medium treated (n = 15 cells from 5 embryos) embryos. (b) Vibration frequency of blastocyst cavity in control (n= 28 embryos) and hypertonic medium treated (n = 18 embryos) embryos. (c) Movement trajectory of Pdgfrα-GFP positive cells in control and hypertonic medium treated embryos. The yellow dotted line denotes the boundary of the cavity. The image on the right is a magnification of the red frame area of the left image. Scale bar, left 25 μm, right 5 μm. Time bar (Lower right), 0 ~ 30 min. (d) Quantification of the distance of the Pdgfrα-GFP positive cells to the center of the ICM surface over time in control and hypertonic medium treated embryos (thin lines are traces of individual cell, thick line is traces of the average of cells, dots are averages, n = 5 cells). (e) Vibration frequency of blastocyst cavity in control and Aphidicolin-treated embryos (n = 10

embryos). (f) Time-lapse (left, Scale bar, 20 μm) and movement trajectory (right, Scale bar, 5 μm. Time bar, 0 ~ 3 h.) of Pdgfrα-GFP positive cells in control and Aphidicolin-treated embryos. The yellow dotted line denotes the boundary of the cavity. The image on the right is a magnification of the red frame area of the left image. (g) Quantification of the distance of the Pdgfrα-GFP positive cells of the control (green, n = 3 embryos) and the Aphidicolin treatment (purple, n = 3 embryos) to the center of the ICM surface over time (thin lines are traces of individual embryo, thick line is traces of the average of embryos). (h) The representative heat map of the velocity field in ICM of control and Aphidicolin-treated embryos analyzed by PIV. The yellow dotted line denotes the boundary of ICM. Scale bar, 20 μm. (i) The statistical analysis of cell speed (rms velocity) of ICM compartment measured by PIV in control (n = 5 embryos) and Aphidicolin-treated embryos (n = 4 embryos). (j) Schematic diagram of the process of hypertonic treatment of blastocysts. The length of the arrow represents the duration of embryo culture. (k) Time-lapse images of embryos expressing Pdgfrα-GFP in control and hypertonic treatment. The yellow dotted line denotes the boundary of the cavity. Scale bar, 20 μm. (l) Quantification of the distance of the Pdgfrα-GFP positive cells to the center of the ICM surface over time in the control (n = 6 cells from 2 embryos) and the hypertonic medium treated (n = 9 cells from 3 embryos) embryos. The experiments were repeated for at least three times.

Figure 3

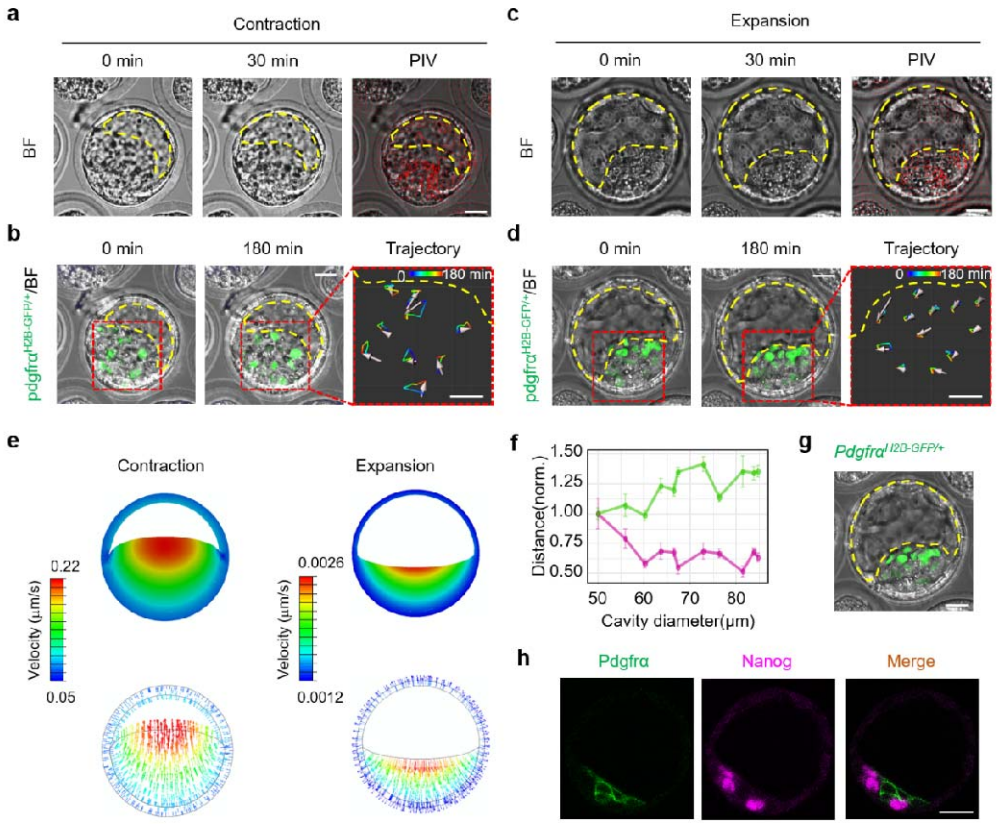

Figure 3. Embryo vibration induces dynamic tissue flow in ICM to drive cell movement (a) The velocity field of ICM compartment during blastocyst contraction analyzed by PIV. The length and direction of the arrow indicate the magnitude and direction of the speed at that point, respectively. The yellow dotted line denotes the boundary of the cavity. (b) Movement trajectory of Pdgfrα-GFP positive cells during contraction of blastocyst. The image on the right is a magnification of the red frame area of the left image. The yellow dotted line denotes the boundary of the cavity. The white arrow indicates the displacement of the cell. Scale bar, 5 μm. Time bar (Upper right), 0 ~ 180 min. (c) The velocity field of ICM compartment during blastocyst expansion analyzed by PIV. The length and direction of the arrow indicate the magnitude and direction of the speed at that point, respectively. The yellow dotted line denotes the boundary of the cavity. (d) Movement trajectory of pdgfrα-GFP positive cells during expansion of blastocyst. The image on the right is a magnification of the red frame area of the left image. The yellow dotted

line denotes the boundary of the cavity. The white arrow indicates the displacement of the cell. Scale bar, 5 μm. Time bar (Upper right), 0 ~ 180 min. (e) A simulation of motion pattern of embryo during contraction and expansion with a simplified finite element model. Images selected to show the distribution of velocity magnitude (top) and orientation (bottom) at the 60 s of contraction (left) and 3600 s of expansion (right). (f) Quantification of the distance of the $Nanog^{+}$/$Nanog^{+}$ cells (magenta) and Pdgfrα⁺/Pdgfrα⁺ cells (green) in blastocyts with different cavity diameters (n = 11 embryos). (g) Representative $Pdgfr\alpha^{H2B\text{-}GFP/+}$ embryo image (right) of the Pdgfrα-GFP positive cells enriched as an “inverted pyramid” at the central region of ICM/cavity boundary. The yellow dotted line denotes the boundary of the cavity. Scale bar, 20 μm. (h) Representative immunofluorescence images of Pdgfrα and Nanog in embryo at “inverted pyramid” intermediate state. Scale bar, 25 μm. The experiments were repeated for at least three times.

Figure 4

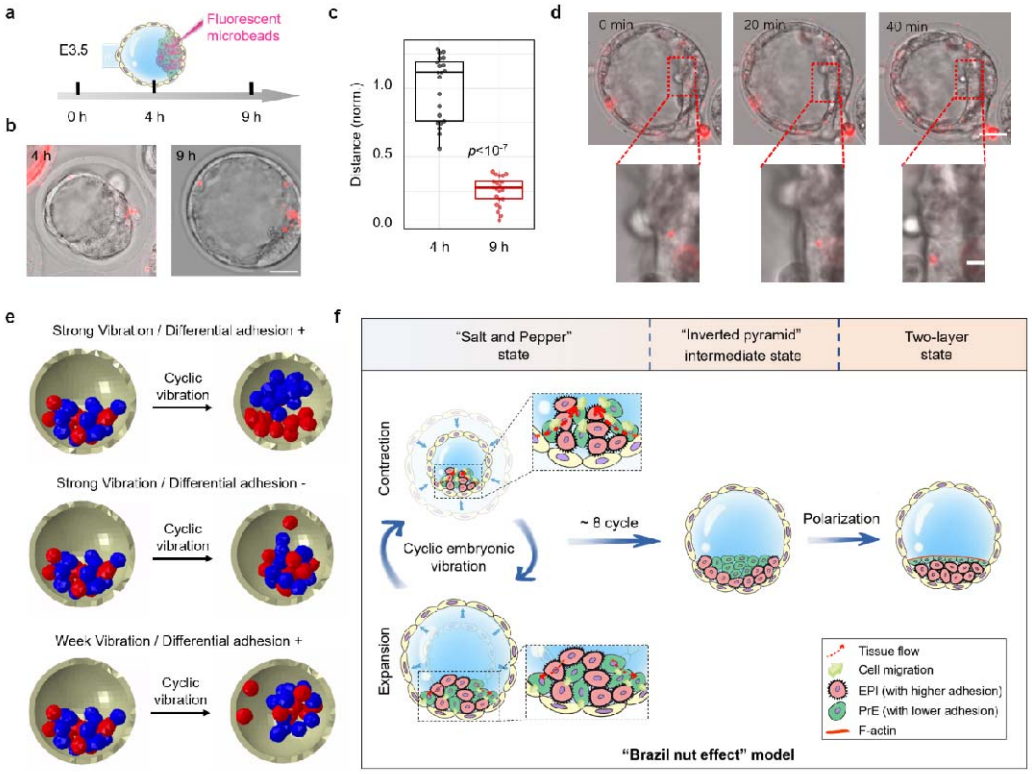

Figure 4. Blastocyst vibration promotes the spatial segregation of PrE/EPI precursor cells through "Brazil nut effect" mechanism (a) Schematic diagram of fluorescent microbeads injection into ICM compartment at E3.5. (b) Representative images of 0 h and 5 h after injection of fluorescent beads in E3.5 embryos. Scale bar, 25 μm. (c) The distance of the fluorescent beads to the center of the ICM surface (n = 21 fluorescent beads from 7 embryos). (d) Representative time-lapse images of fluorescent beads movement in ICM. The bottom images are an enlarged view of the red box areas of the top images. Scale bar, top: 25 μm, bottom: 5 μm. (e) A Simulations of cell viscous segregation during embryo vibration with a simplified finite element model. The model was to illustrate the effect of cohesive properties and periodic contraction-expansion of embryos on the separation of PrE and EPI cells. Top: The separation process of PrE and EPI cells with different cohesive properties (EPI: red, strong cohesiveness; PrE: blue, week cohesiveness) under periodic embryo contraction-expansion. Middle: The separation

failed when cohesive properties of cells were the same. Bottom: The separation failed when embryo contraction speed reduced to one-third. (f) “Brazil nut effect” model of the ICM segregation. The experiments were repeated for at least three times.

Figure 5

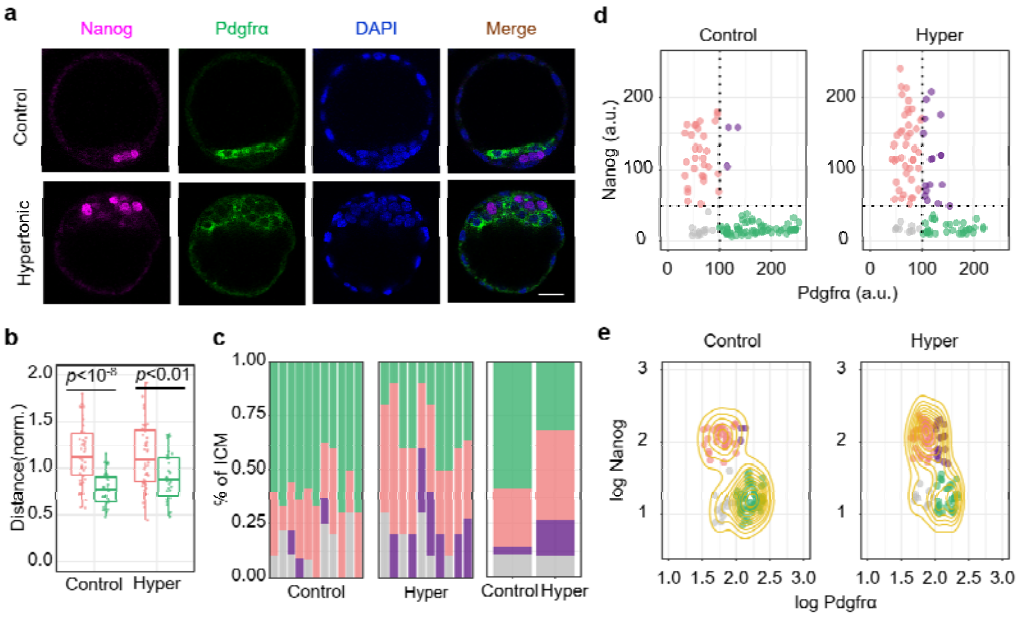

Figure 5. Hypertonic treatment inhibits the spatial segregation and lineage specification of PrE/EPI (a) Representative immunofluorescence images of the E3.5 embryos fixed after 24 hours of culture in hypertonic or normal medium (Control). Scale bar, 25 μm. (b) The distance of Nanog and Pdgfrα positive cells to the center of the ICM surface in control (Nanog: n = 46 cells from 9 embryos, Pdgfrα: n = 33 cells from 9 embryos) and hypertonic treatment (Hyper, Nanog: n = 49 cells from 7 embryos, Pdgfrα: n = 30 cells from 7 embryos). (c) Average ICM composition at the end of the culture period in normal or hypertonic medium, shown as % of the ICM. DN, gray, double negative (Nanog-, Pdgfrα-); DP, purple, double positive (Nanog+, Pdgfrα+); EPI, red, (Nanog+, Pdgfrα-); PrE, green, (Nanog-, Pdgfrα-). Comtrol: n = 108 cells from 11 embryos. Hypertonic: n = 101 cells from 10 embryos. (d) Scatter plot of fluorescence intensity levels of Nanog and Pdgfrα after hypertonic treatment. (e) Scatter plots for same data as in (d), represented as logarithm. The yellow contour lines show the density. The experiments were repeated for at least three times.

Figure 6

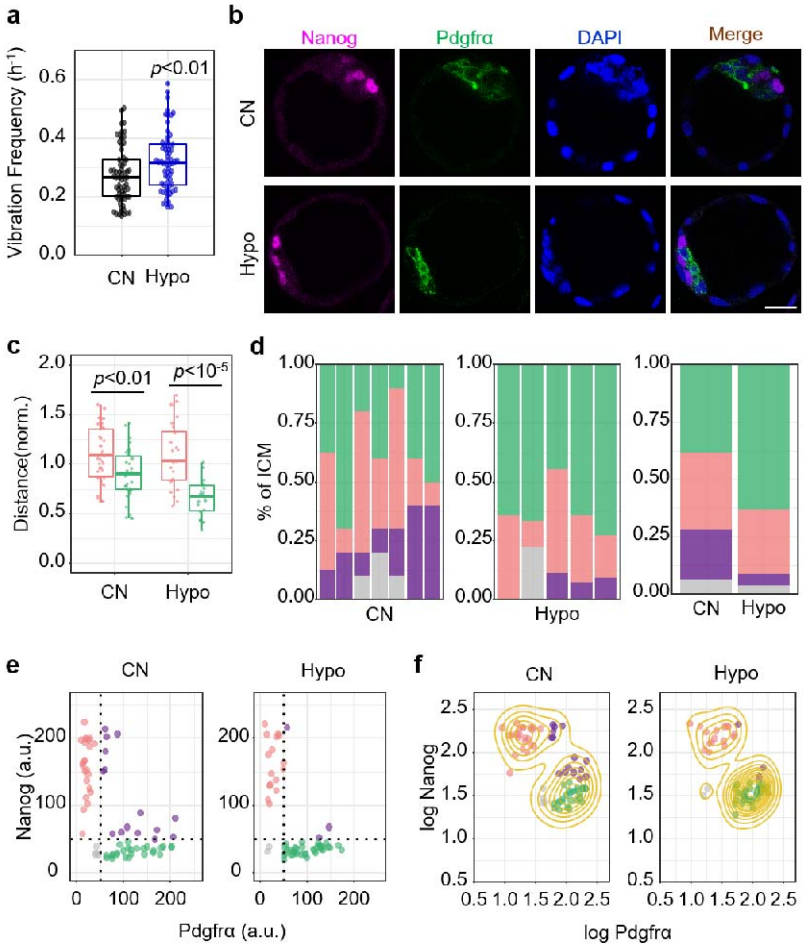

Figure 6. Hypotonic treatment promotes the spatial segregation and lineage specification of PrE/EPI (a) Vibration frequency of blastocyst cavity in control (CN, n = 66 embryos) and hypotonic-treated (Hypo, n = 64 embryos) embryos. (b) Representative immunofluorescence images of the E3.25 embryos fixed after 24 hours of culture in hypertonic or normal medium. Scale bar, 25 µm. (c) The distance of Nanog and Pdgfrα positive cells to the center of the ICM surface in control (Nanog: n = 41 cells from 8 embryos, Pdgfrα: n = 35 cells from 8 embryos) and hypotonic treated (Nanog: n = 24 cells from 5 embryos, Pdgfrα n = 21 cells from 5 embryos) embryos. (d) Average ICM composition at the end of the culture period in embryos treated with normal or hypotonic medium, shown as % of the ICM. (e) Scatter plot of fluorescence intensity levels of Nanog and Pdgfrα after hypotonic treatment. DN, gray, double negative (Nanog-, Pdgfrα-); DP, purple, double positive (Nanog+, Pdgfrα+); EPI, red, (Nanog+, Pdgfrα-); PrE, green, (Nanog-,

Pdgfrα-). Comtrol: n = 68 cells from 7 embryos. Hypotonic: n = 57 cells from 5 embryos. (f) Scatter plots for same data as in (e), represented as logarithm. The yellow contour lines show the density. The experiments were repeated for at least three times.

Figure 7

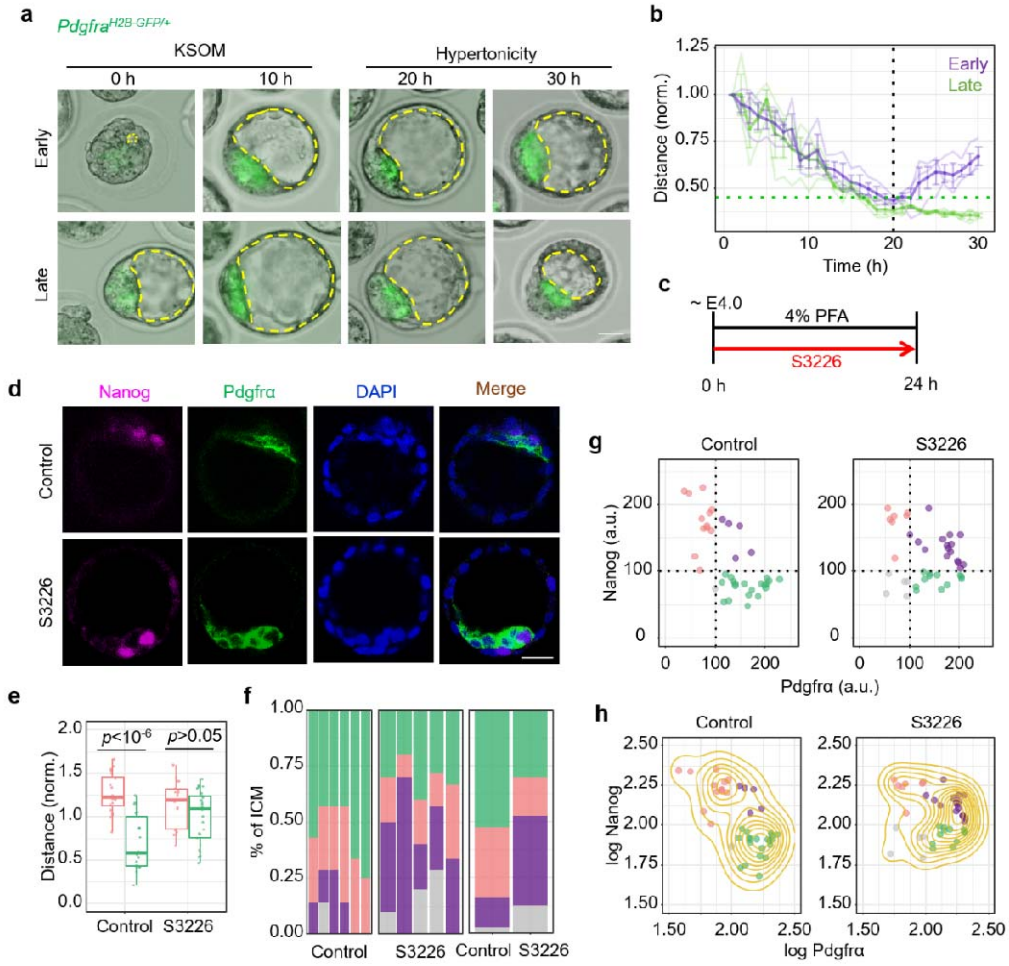

Figure 7. PrE/EPI spatial segregation and lineage specification maintenance requires embryo vibration during the initial stage after two-layer pattern formation (a) Representative time-lapse images of blastocysts expressing Pdgfrα-GFP in control and hypertonic medium at early or late stage. The yellow dotted line denotes the boundary of the cavity. Scale bar, 25 μm. (b) Quantification of the distance of the Pdgfrα-GFP positive cells to the center of the ICM surface over time in embryos treated with hypertonicity at early or late stage (n = 3 embryos, thin lines are traces of individual embryo, thick line is traces of the average of embryos). (c) Schematic diagram of the process of S3226 treatment of blastocysts. The length of the arrow represents the duration of embryo culture. (d) Representative immunofluorescence images of the E4.0 embryos treated with

S3226 as (c). Scale bar, 25 μm. (e) The distance of Nanog and Pdgfrα positive cells to the center of the ICM surface in control (Nanog: n = 20 cells from 4 embryos, Pdgfrα: n = 18 cells from 4 embryos) or S3226-treated (Nanog: n = 19 cells from 4 embryos, Pdgfrα: n = 25 cells from 4 embryos) embryos. (f) Average ICM composition at the end of the culture period in control or S3226-treated embryos, shown as % of the ICM. Comtrol: n = 38 cells from 6 embryos. S3226: n = 40 cells from 5 embryos. (g) Scatter plot of fluorescence intensity levels of Nanog and Pdgfrα in control or S3226-treated embryos. DN, gray, double negative (Nanog-, Pdgfrα-); DP, purple, double positive (Nanog+, Pdgfrα+); EPI, red, (Nanog+, Pdgfrα-); PrE, green, (Nanog-, Pdgfrα-). (h) Scatter plots for same data as in (g), represented as logarithm. The yellow contour lines show the density. The experiments were repeated for at least three times.

Figure 8

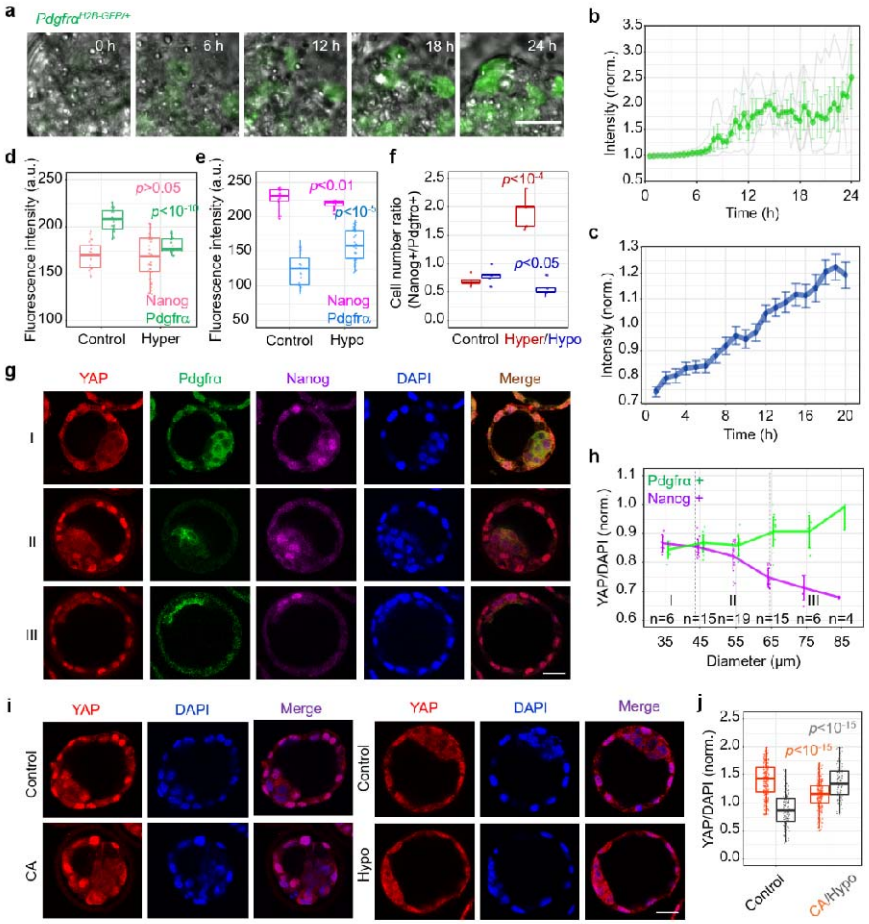

Figure 8. Periodic embryo vibration regulates gene expression of EPI and PrE precursors by YAP (a) Representative time-lapse images of the ICM in a pdgfrα-GFP expressing embryo during develpment. Scale bar, 20 μm. (b) Quantification of the fluorescence intensity of Pdgfrα-GFP positive cells in a representative single embryo over time ((n = 4 Pdgfrα-GFP positive cells, thin lines are traces of individual cell, thick line is traces of the average of cells). (c) Quantification of the fluorescence intensity of Pdgfrα-GFP positive cells in multiple embryos over time. n = 13 embryos. (d) The fluorescence intensity of control (Nanog: n = 22 cells from 5 embryos, Pdgfrα: n = 31 cells from 5 embryos) and hypertonicity-treated (Nanog: n = 34 cells from 5 embryos, Pdgfrα: n = 18 cells from 5 embryos) embryos. (e) The fluorescence intensity of control (Nanog: n = 18 cells from 5 embryos, Pdgfrα: n = 23 cells from 5 embryos) and hypotonicity-treated (Nanog: n = 18 cells from 5 embryos, Pdgfrα: n = 33cells from 5 embryos) embryos. (f) The cell number ratio of

Nanog^{+}/Pdgfrα^{+} in control, hypertonicity or hypotonicity treated embryos. (g) Representative immunofluorescence images of blastocysts at different stages. Scale bar, 25 μm. (h) Quantification of the YAP/DAPI fluorescence intensity in Nanog+ cells and Pdgfrα+ cells in embryos different cavity diameters. (i) Representative immunofluorescence images of E3.5 embryos treated with CA or hypotonicity. Scale bar, 25 μm. (j) The statistical analysis of YAP/DAPI fluorescence intensity of ICM cells in embryos treated with CA (Control: n = 304 cells from 17embryos, CA: n = 304 cells from 15 embryos) or hypotonicity (Control: n = 147 cells from 8 embryos, Hypotonicity n = 108 cells from 7 embryos). The experiments were repeated for at least three times.

Figure 9

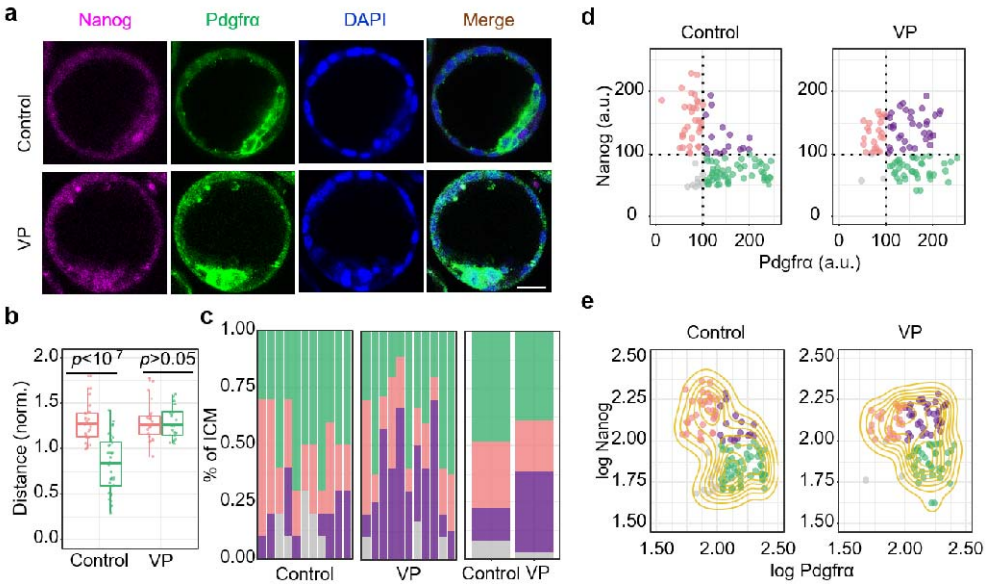

Figure 9. YAP inhibition prevents the spatial segregation and lineage specification of PrE/EPI (a) Representative immunofluorescence images of the E3.5 embryos fixed after 24 hours of VP treatment. Scale bar, 25 μm. (b) The distance of Nanog and Pdgfrα positive cells to the center of the ICM surface in control (Nanog: n = 27 cells from 7 embryos, Pdgfrα: n = 36 cells from 7 embryos) or VP treated (Nanog: n = 23 cells from 5 embryos, Pdgfrα: n = 23 cells from 5 embryos) embryos. (c) Average ICM composition at the end of the culture period in control or VP-treated embryos, shown as % of the ICM. Comtrol: n = 110 cells from 11 embryos. VP: n = 98 cells from 11 embryos. (d) Scatter plot of fluorescence intensity levels of Nanog and Pdgfrα after VP treatment. DN, gray, double negative (Nanog -, Pdgfrα-); DP, purple, double positive (Nanog +, Pdgfrα+); EPI, red, (Nanog +, Pdgfrα-); PrE, green, (Nanog -, Pdgfrα-). (e) Scatter plots for same data as in (d), represented as logarithm. The yellow contour lines show the density. The experiments were repeated for at least three times.

SUPPLEMENTARY MATERIALS

Supplementary Figures

Supplementary Figure1

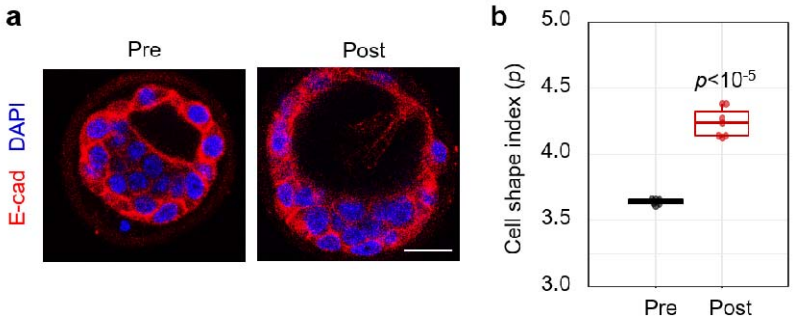

Supplementary Figure 1. The shape index of ICM cells pre and post the emergence of rhythmic embryo vibration (a) Representative immunofluorescence images of embryos pre and post the emergence of rhythmic embryo vibration. Cell shape is indicated by E-cadherin (E-cad) labeling. Scale bar, 25 μm. (b) The shape index of cells in ICM pre (n = 6 embryos) and post (n = 7 embryos) the emergence of rhythmic embryo vibration. The dot represents the mean value of the shape index of the cells in the ICM of an embryo. The experiments were repeated for at least three times.

Supplementary Figure 2

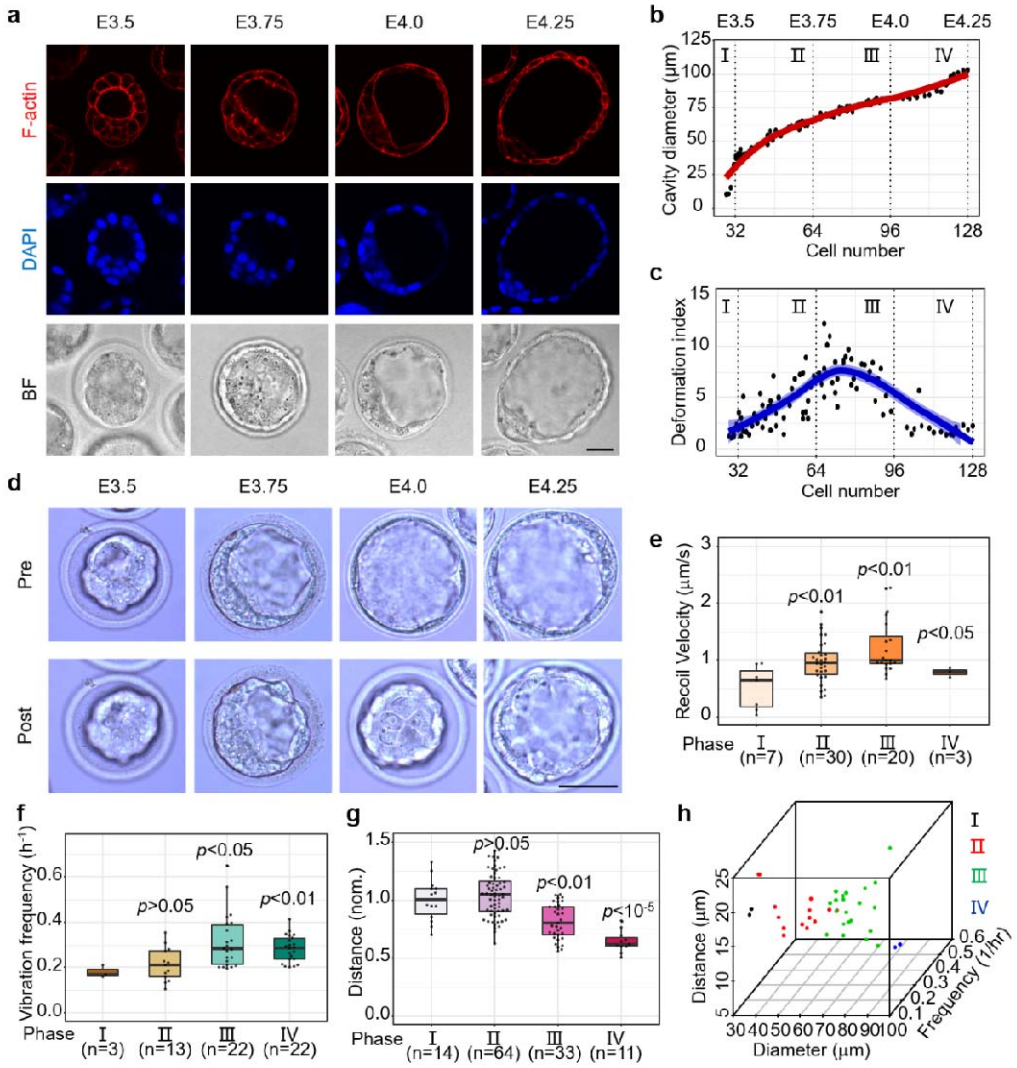

Supplementary Figure 2. Migration of PrE precursors is correlated with tension and vibration of blastocysts at different stages (a) Representative immunofluorescence and bright field images of blastocysts at different stages. F-actin is stained by Phalloidin. Scale bar, 25 μm. (b) Quantification of the cavity diameter of embryos with different cell numbers. The dots indicate the cavity diameter of an embryo. The line represents the local linear regression fitting curve of the cavity diameter of multiple embryos. The dotted lines denote the 4 phases segmented according to cortical tension n = 99 embryos. (c) Quantification of the TE cells deformation index (aspect ratio)

of embryos with different cell numbers. The dots indicate the TE cells deformation index of an embryo. The line represents the local linear regression fitting curve of the TE cells deformation index of multiple embryos. n = 99 embryos. (d) The images of embryos at different stages indicating the cavity recoil post UV laser cutting. Scale bar, 50 μm. (e) The cavity recoil speed after UV laser cut of embryos at different stages**.** (f) The vibration frequency of the blastocyst cavity of embryos at different phases. (g) The distance of the Pdgfrα-GFP positive cells to the center of the ICM surface in embryos at different stages. (h) The correlation of cavity diameter, vibration frequency and the distance of Pdgfrα-GFP positive cells to the center of the ICM surface. n = 41 embryos. The experiments were repeated for at least three times.

Supplementary Figure 3

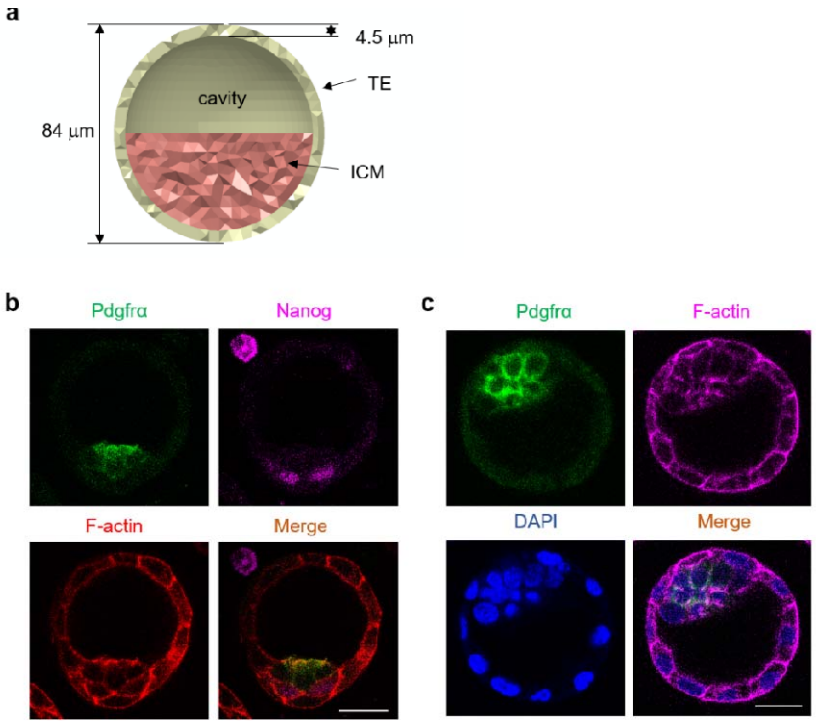

Supplementary Figure 3. Mechanical model and F-actin assembly in blastocysts (a) The cross-section of the finite element model in Figure 4e. (b) Representative immunofluorescence images of embryos with the Pdgfrα-GFP positive cells showing "inverted pyramid" distribution. Scale bar, 25 μm. (c) Representative immunofluorescence images of embryos with the outermost Pdgfrα-GFP positive cells showing a “Rose-like” distribution at the surface of ICM. Scale bar, 25 μm. The experiments were repeated for at least three times.

Supplementary Figure 4

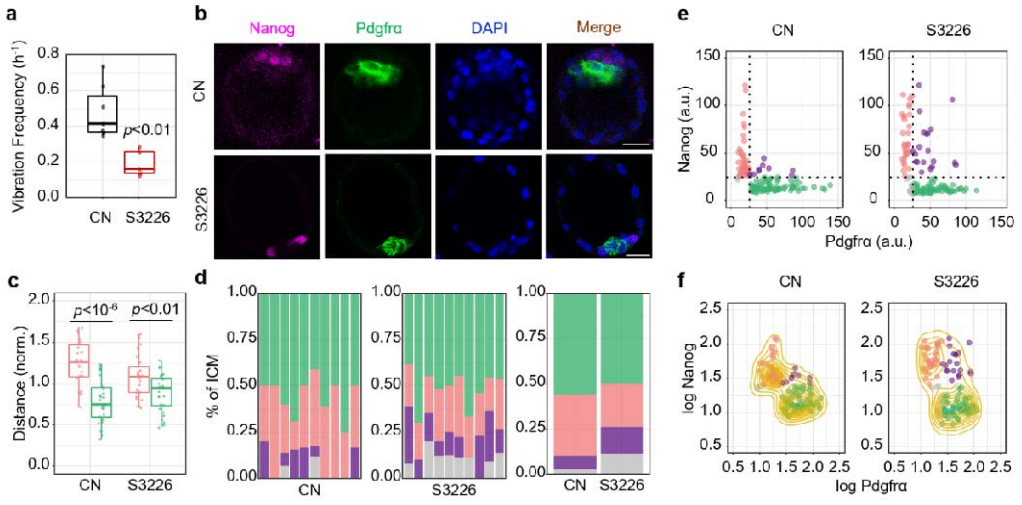

Supplementary Figure 4. S3226 treatment inhibits the spatial segregation and lineage specificaiton of PrE/EPI (a) Vibration frequency of blastocyst cavity in control (CN, n = 7 embryos) and S3226-treated (S3226, n = 5 embryos) embryos. (b) Representative immunofluorescence images of the E3.5 embryos fixed after 24 hours of S3226 treatment. Scale bar, 25 μm. (c) The distance of Nanog and Pdgfrα positive cells to the center of the ICM surface in control (Nanog: n = 23 cells from 7 embryos, Pdgfrα: n = 27 cells from 7 embryos) and S3226 treated (Nanog: n = 29 cells from 7 embryos, Pdgfrα: n = 29 cells from 7 embryos) embryos. (d) Average ICM composition at the end of the culture period for embryos treated with S3226, shown as % of the ICM. Control: n = 129 cells from 10 embryos. S3226: n = 133 cells from 10 embryos. (e) Scatter plot of fluorescence intensity levels of Nanog and Pdgfrα after S3226 treatment. DN, gray, double negative (Nanog -, Pdgfrα-); DP, purple, double positive (Nanog +, Pdgfrα+); EPI, red, (Nanog +, Pdgfrα-); PrE, green, (Nanog -, Pdgfrα-). (f) Scatter plots for same data as in (e), represented as logarithm. The yellow contour lines show the density. The experiments were repeated for at least three times.

Supplementary Figure 5

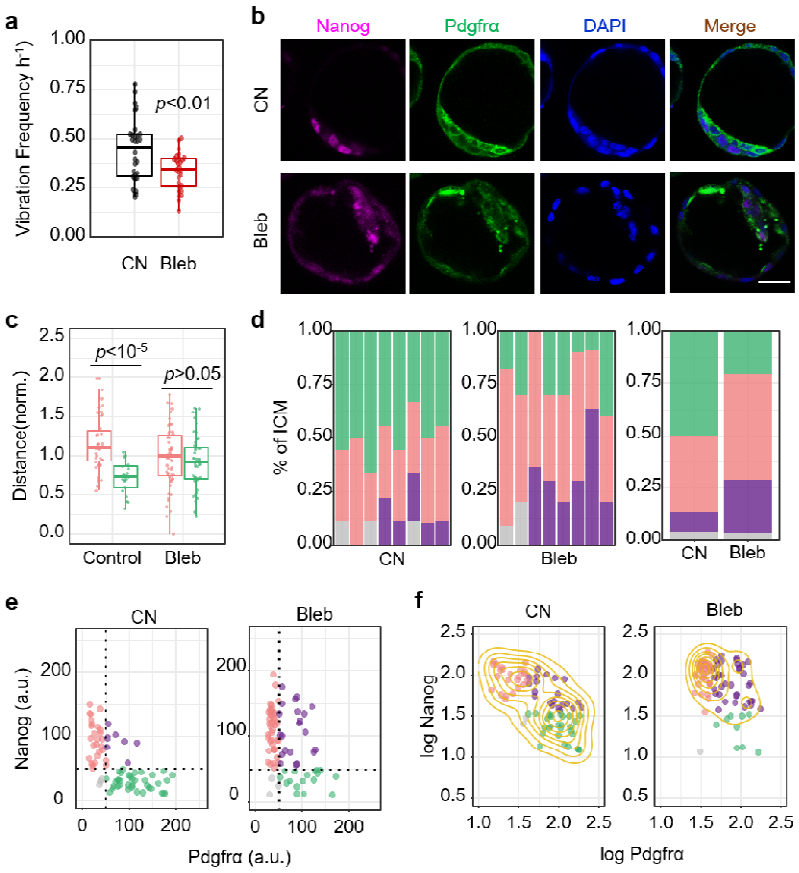

Supplementary Figure 5. Blebbistatin treatment inhibits the spatial segregation and lineage specification of PrE/EPI (a) Vibration frequency of blastocyst cavity in control (CN, n = 30 embryos) and Blebbistatin-treated (Bleb, n = 27 embryos) embryos. (b) Representative immunofluorescence images of the E3.5 embryos fixed after 24 hours of Bleb treatment. Scale bar, 25 μm. (c) The distance of Nanog and Pdfrα positive cells to the center of the ICM surface in control (Nanog: n = 39 cells from 7 embryos, Pdgfrα: n = 21 cells from 7 embryos) and Bleb treated (Nanog: n = 54 cells from 6 embryos, PDGFRα: n = 46 cells from 6 embryos) embryos. (d) Average ICM composition at the end of the culture period for embryos treated with Bleb, shown as % of the ICM. Comtrol: n = 74 cells from 8 embryos. Bleb: n = 83 cells from 8 embryos. (e) Scatter plot of fluorescence intensity levels of Nanog and Pdgfrα after Bleb treatment. DN, gray, double negative (Nanog -, Pdgfrα-); DP, purple, double positive (Nanog +, Pdgfrα+); EPI, red,

(Nanog +, Pdgfrα-); PrE, green, (Nanog -, Pdgfrα-). (f) Scatter plots for same data as in (e), represented as logarithm. The yellow contour lines show the density. The experiments were repeated for at least three times.

Supplementary Figure 6

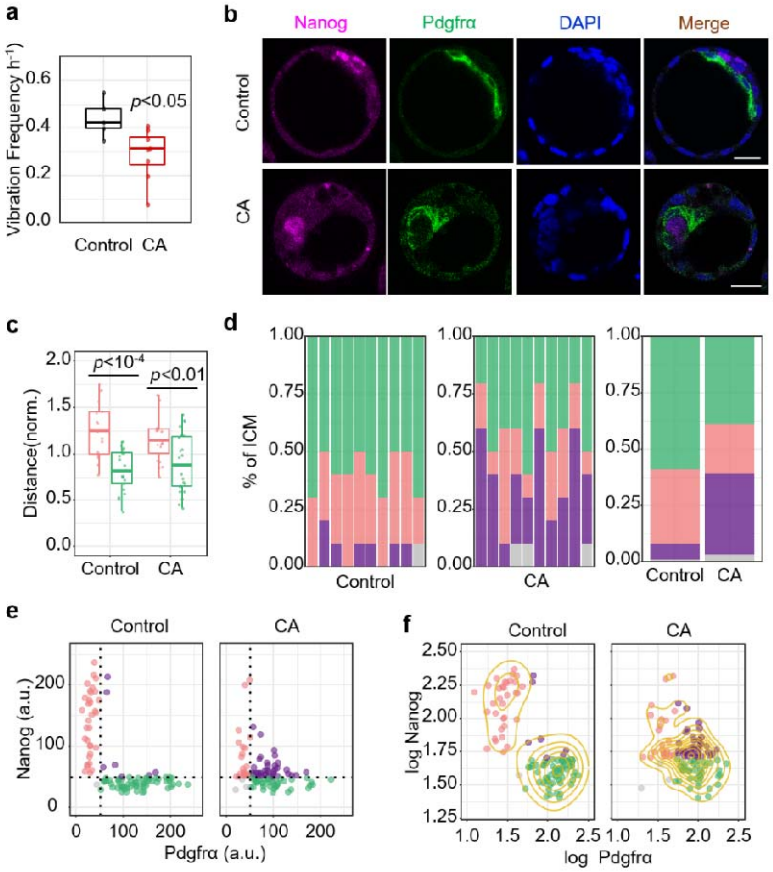

Supplementary Figure 6. Cytochalasin A treatment inhibits the spatial segregation and lineage specification of PrE/EPI layers (a) Vibration frequency of blastocyst cavity in control (Control, n = 5 embryos) and cytochalasin A treatment (CA, n = 8 embryos). (b) Representative immunofluorescence images of the E3.5 embryos fixed after 24 hours of CA treatment. Scale bar, 25 μm. (c) The distance of Nanog and Pdfrα positive cells to the center of the ICM surface in control (Nanog: n = 15 cells from 5 embryos, Pdgfrα: n = 21 cells from 5 embryos) and CA treated (Nanog: n = 19 cells from 5 embryos, Pdgfrα: n = 23 cells from 5 embryos) embryos. (d) Average ICM composition at the end of the culture period for embryos treated with CA, shown as % of the ICM. Comtrol: n = 100 cells from 10 embryos. CA: n = 100 cells from 10 embryos. (e) Scatter plot of fluorescence intensity levels of Nanog and Pdgfrα after CA treatment. DN, gray, double negative (Nanog-, Pdgfrα-); DP, purple, double positive (Nanog+, Pdgfrα+); EPI, red,

(Nanog+, Pdgfrα-); PrE, green, (Nanog-, Pdgfrα-). (f) Scatter plots for same data as in (e), represented as logarithm. The yellow contour lines show the density. The experiments were repeated for at least three times.

Supplementary Figure 7

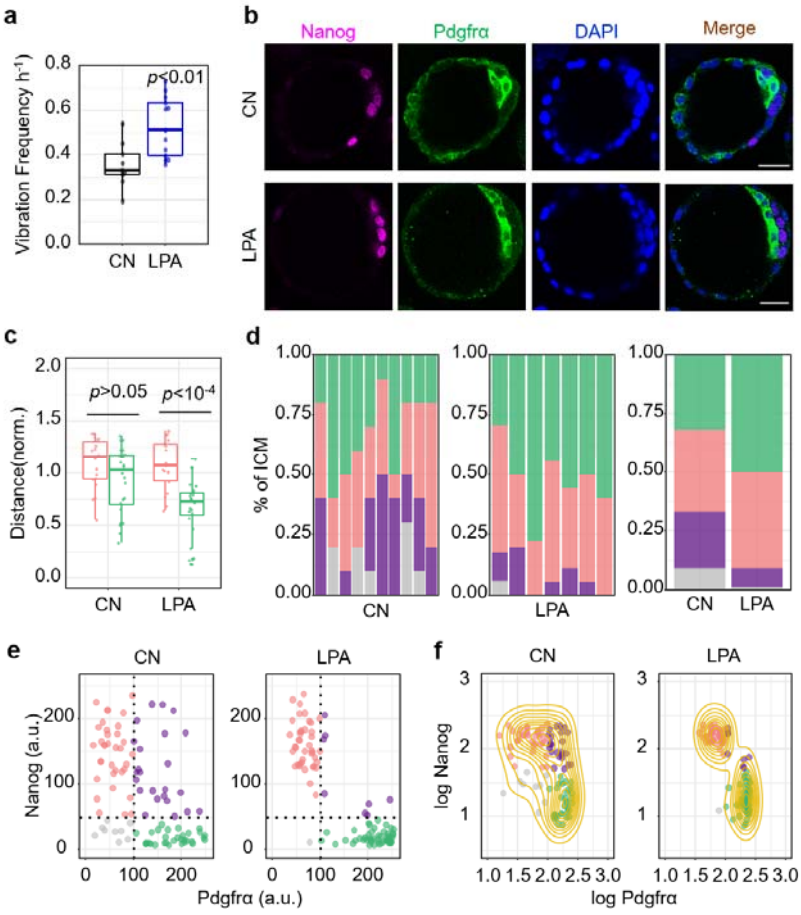

Supplementary Figure 7. LPA treatment facilitates the spatial segregation and lineage specification of PrE/EPI (a) Vibration frequency of blastocyst cavity in control (CN, n = 9 embryos) and LPA treatment (LPA, n = 13 embryos). (b) Representative immunofluorescence images of the embryos fixed after 24 hours of LPA treatment. Scale bar, 25 μm. (c) The distance of Nanog and Pdgfrα positive cells to the center of the ICM surface in control (Nanog: n = 18 cells from 5 embryos, Pdgfrα: n = 24 cells from 5 embryos) and LPA-treated (Nanog: n = 17 cells from 5 embryos, Pdgfrα: n = 23 cells from 5 embryos) embryos. (d) Average ICM composition at the end of the culture period for embryos treated with LPA, shown as % of the ICM. Comtrol: n = 100 cells from 10 embryos. LPA: n = 100 cells from 7 embryos. (e) Scatter plot of fluorescence intensity levels of Nanog and Pdgfrα after LPA treatment. DN, gray, double negative (Nanog-, Pdgfrα-); DP, purple, double positive (Nanog+, Pdgfrα+); EPI, red, (Nanog +, Pdgfrα-); PrE, green,

(Nanog -, Pdgfrα-). (f) Scatter plots for same data as in (e), represented as logarithm. The yellow contour lines show the density. The experiments were repeated for at least three times.

Supplementary Figure 8

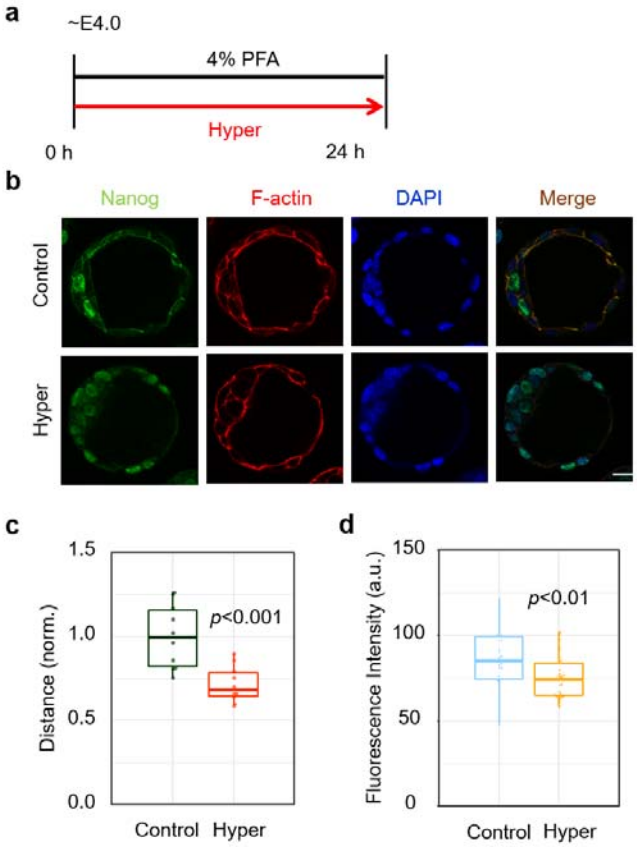

Supplementary Figure 8. Hypertonic treatment reverses the spatial segregation and lineage specification of PrE/EPI (a) Schematic diagram of the process of hypertonic treatment of blastocysts. The length of the arrow represents the duration of embryo culture. (b) Representative immunofluorescence images of embryos treated as indicated in (a). Scale bar, 25 μm. (c) The distance of the Nanog positive cells to the center of the ICM surface. n = 10 cells from 2 embryos. (d) The fluorescence intensity of Nanog positive cells in control and hypertonicity-treated embryos. n = 30 cells from 6 embryos. The experiments were repeated for at least three times.

Supplementary Figure 9

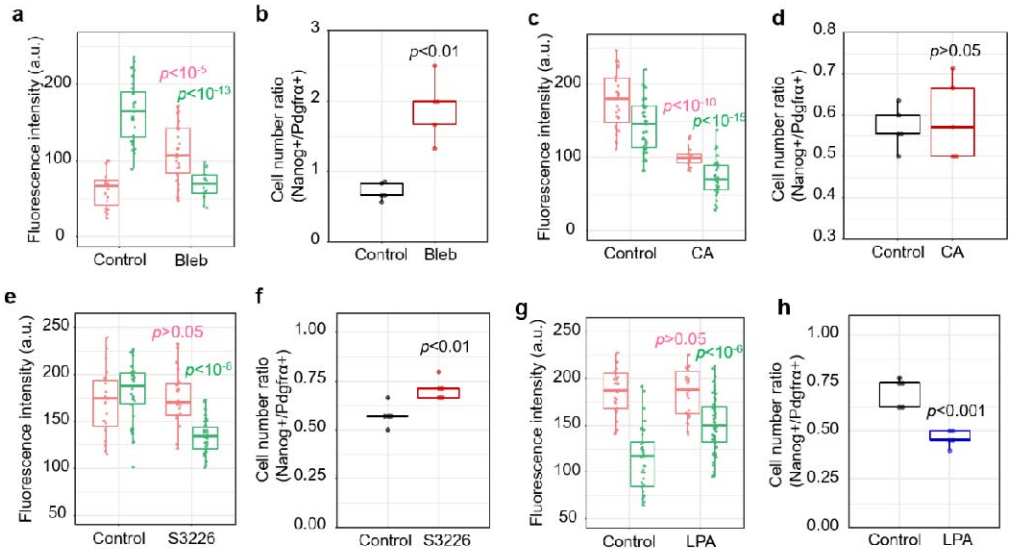

Supplementary Figure 8. Gene expression pattern of ICM cells in each treatment group (Bleb, CA, S3226, and LPA) (a) The fluorescence intensity of control (Nanog: n = 23 cells from 5 embryos, Pdgfrα: n = 32 cells from 5 embryos) and Bleb-treated (Nanog: n = 26 cells from 5 embryos, Pdgfrα: n = 14 cells from 5 embryos) embryos. (b) The cell number ratio (Nanog+/Pdgfrα+) of control and Bleb-treated embryos in ICM. The same data as in (a). (c) The fluorescence intensity of control (Nanog: n = 27 cells from 5 embryos, Pdgfrα: n = 47 cells from 5 embryos) and CA-treated (Nanog: n = 22 cells from 5 embryos, Pdgfrα: n = 37cells from 5 embryos) embryos. (d) The cell number ratio (Nanog+/Pdgfrα+) of control and CA-treated embryos in ICM. The same data as in (c). (e) The fluorescence intensity of control (Nanog: n = 19 cells from 5 embryos, Pdgfrα: n = 33 cells from 5 embryos) and S3226-treated (Nanog: n = 22 cells from 5 embryos, Pdgfrα: n = 31 cells from 5 embryos) embryos. (f) The cell number ratio (Nanog+/Pdgfrα+) of control and S3226-treated embryos in ICM. The same data as in (e). (g) The fluorescence intensity of control (Nanog: n = 29 cells from 5 embryos, Pdgfrα: n = 41cells from 5 embryos) and LPA-treated (Nanog: n = 26 cells from 5 embryos, Pdgfrα: n = 56 cells from 5 embryos) embryos. (h) The cell number ratio (Nanog +/Pdgfrα+) of control and LPA-treated embryos in ICM. The same data as in (g). The experiments were repeated for at least three times.

Supplementary Movies

Movie S1. Approach of PrE Cells to the Center of the ICM Surface, Related to Figure 1b

Imaging live embryo expressing *Pdgfrα*$^{H2B\text{-}GFP/+}$ shows that the relative allocation of Pare cells tended to approach to the center of ICM surface after E3.75. The scale bar is 20 μm. Time is indicated in h.

Movie S2. Rhythmic Vibration of the Embryo, Related to Figure 1f

Live-imaging of an embryo shows that the blastocyst cavity continues to expand until E3.75, after which the blastocyst begins to display rhythmic vibration. Each contraction is marked in the upper right corner of the video. The scale bar is 20 μm. Time is indicated in h.

Movie S3. Phase Change of ICM, Related to Figure 1h

Movie shows the heat map of the velocity field during embryonic development. At about 9h, the ICM undergoes a phase change from solid-like to liquid-like. The scale bar is 20 μm. The color bar of the heat map is 0 ~ 9 μm/h. Time is indicated in h.

Movie S4. Hypertonic Treatment Inhibits Cell Motility, Related to Figure 2c

(a) Movie shows the movement of PrE cells in a live embryo expressing *pdgfrα*$^{H2B\text{-}GFP/+}$. (b) Movie shows live embryo treated with hypertonicity, which indicates that hypertonic treatment can significantly inhibit cell movement. The scale bar is 20 μm. Time is indicated in h.

Movie S5. Direction of the Cell Movement during the Contraction of Embryo, Related to Figure 3b

Live-imaging of an embryo expressing *pdgfrα*$^{H2B\text{-}GFP/+}$ shows that the movement of PrE cells during contraction is towards the center of the ICM, demonstrating the consistency of tissue flow and the movement direction of PrE cells. The scale bar is 20 μm. Time is indicated in h.

Movie S6. Direction of the Cell Movement during the Expansion of Embryo, Related to Figure 3d

Live-imaging of an embryo expressing *pdgfrα*$^{H2B\text{-}GFP/+}$ indicates that during the expansion of blastocoel, the direction of tissue flow is paralleled with the ICM/cavity boundary. The scale bar is 20 μm. Time is indicated in h.

Movie S7. Simulations of 10% embryo contraction and expansion with a simplified continuous model, Related to Figure 3e

The model was to illustrate the trend of velocity vector distribution during contraction and expansion.

a. Distribution of velocity magnitude in contraction from 0-60s.

b. Distribution of velocity orientation in contraction from 0-60s.

c. Distribution of velocity magnitude in expansion from 0-3600s.

d. Distribution of velocity orientation in expansion from 0-3600s.

Movie S8. Movement of Microbeads after Embryo Contraction, Related to Figure 4d

Imaging live embryo injected with fluorescent microbeads shows the movement of microbeads after embryo contraction. The scale bar is 20 μm. Time is indicated in min.

Movie S9. Simulations of cell viscous segregation during embryo vibration with a simplified finite element model, Related to Figure 4e

The model was to illustrate the effect of cohesive properties and periodic contraction-expansion of embryos on the separation of PrE and EPI cells.

a. The separation process of PrE and EPI cells with different cohesive properties (EPI: red, strong cohesiveness; PrE: blue, week cohesiveness) under periodic embryo contraction-expansion.

b. The separation failed when cohesive properties of cells were the same.

c. The separation failed when embryo contraction speed reduced to one-third.

Movie S10. Regulation of Gene Expression, Related to Figure 8a

Live-imaging of an embryo expressing *pdgfrα*$^{H2B\text{-}GFP/+}$ indicates that during the migration of Pdgfra positive cells, GFP expression intensity gradually increased. The scale bar is 20 μm. Time is indicated in h.

Mechanical Modeling

To assess the motion pattern of the embryo compound during contraction and expansion, a simplified continuous model was developed. As shown in Supplementary Fig. S2a, the model consist of TE, ICM, and the cavity. The geometric information of the model was based on the microscope images of the embryo. The embryo was assumed to be isotropic material with the modulus of 360 Pa, poisson ratio of 0.45, and density of 1000 kg/m^3. The model was meshed with 4-node linear tetrahedron in the approximate size of 4 μm. A contraction of 10% diameter in 2 minutes and an expansion of 10% diameters in 2 hours was simulated. The distributions of velocity magnitude and orientation were shown in Fig. 3e.

To study the effect of cohesive properties and periodic contraction-expansion of embryo on the separation of PrE and EPI cells, a simplified finite element model of embryo was developed (Figure 4h). The geometric information of the model was based on the microscope images of the embryo. The embryo was simplified as a sphere with the diameter of 84 μm. PrE and EPI cells were simplified as spheres with the diameter of 13 μm. Material property of all cells was assumed to be isotropic with the elastic modulus of 360 Pa, poisson ratio of 0.45, and density of 1000 kg/m^3. A liquid damping coefficient of $9.4e^{-11}$ MPa*s was applied. The model was meshed with 4-node linear tetrahedron in the approximate size of 5 μm. To accelerate the simulation, the periods of contraction and expansion was set to 0.36 s and 0.54 s, and a mass scaling acceleration algorithm was applied. 7 cycles were simulated. Since the real expansion was a quasi-static process, the kinetic energy was set to 0 at the beginning of each cycle. The cohesive properties between PrE, EPI, and TE cells were assumed to be different (Table 1). To study the effect of different cohesive properties on the separation of PrE and EPI cells, a control case with the same cohesive property (= Y-Z cohesive property) was developed. To study the effect of different contraction speed on the separation of PrE and EPI cells, a control case with the contraction speed 3 times slower was developed (Figure 4h).

Table 1: Cohesive stiffness coefficient between PrE, EPI, and TE cells

Cell type	Normal	Tangential
PrE-PrE	$5e^{-5}$	$1.0e^{-11}$
PrE-EPI	$1.7e^{-6}$	$7.2e^{-13}$
EPI-EPI	$7.2e^{-5}$	$2.0e^{-10}$
PrE-TE	$1e^{-7}$	$1.0e^{-13}$
EPI-TE	$6e^{-5}$	$6.6e^{-8}$

MATERIALS AND METHODS

Mouse Husbandry

All mice were bred and reared in the animal facility of Tsinghua University at 22 °C with a 12-hour light/dark cycle (lighting time 7:00-19:00). Food and water are freely available. All animal studies were conducted under the guidance of the Animal Care and Utilization Committee (IACUC) of Tsinghua University. According to the National Institutes of Health "Animal Ethical Use Guidelines", the experimental procedure has been approved by the Laboratory Animal Care and Use Management Committee of Tsinghua University and the Beijing Municipal Science and Technology Commission (SYXK- 2019-0044).

Embryo Collection and Culture

In order to obtain preimplantation embryos, female mice (2～3 months old) were injected intraperitoneally with 10 international units (IU) of pregnant mare serum gonadotropin, and then injected with 10 international units (IU) of human chorionic gonadotropin (hCG; 48 hours later. After the injection of hCG, the female mice in the superovulation period were directly mated with male mice (3～4 months old). The pre-implanted embryo was flushed out of the uterus or fallopian tube with KSOM. Then Embryos were cultured in drops of KSOM under mineral oil (Sigma) at 37 □ in a 5% CO_2 atmosphere.

Pharmacological Treatment

Sucrose was resuspended in ddH_2O, the concentration of the stock solution was 1 mol/L. The stock concentration of 100 mM was diluted in KSOM (260 mOsm) into a hypertonic solution (340 mOsm). We used ddH_2O to dilute KSOM into a 70% hypotonic solution (170 mOsm). Blebbistatin was resuspended in DMSO at a concentration of 25 mM. Then we diluted the stock solution in KSOM to a working concentration of 1 μM. Resuspend Cardamonin in DMSO at the stock concentration of 20 mg/mL. For a working concentration of 20 μg/mL, the stock concentration was diluted in KSOM. Resuspend LPA in methanol at the stock concentration of 1

mM. The stock solution was diluted by KSOM to a working concentration of 5 μM. CA was resuspended in DMSO at the stock concentration of 0.5 mg/mL. The stock solution was diluted by KSOM to a working concentration of 1 μg/mL. We resuspended S3226 in DMSO to prepare a stock solution with a concentration of 2 mg/mL. The stock solution was diluted by KSOM to a working concentration of 20 nM. Resuspend VP in DMSO to prepare a stock solution with a concentration of 10 mg/mL. The stock solution was diluted by KSOM to a working concentration of 2 μg/mL.

Live Embryo Imaging

For real-time imaging, embryos were cultured in 20 μL of KSOM drops covered with 2 mL of mineral oil on a 35 mm glass bottom dish in an environmental chamber at 37 °C with 5% CO_2.

Embryo immunofluorescence staining

Embryos were washed in Dulbecco's phosphate buffered saline (DPBS) containing 1% (w/v) polyvinylpyrrolidone (PVP) and fixed with 4% PFA for 15 minutes at room temperature, then infiltrated with DPBS (0.5% Triton-100), placed at room temperature for 20 minutes, and then transferred to blocking buffer (DPBS containing 0.1% Tween-20) at 4°C; 3% BSA) for at least 4 hours. The embryos were incubated with primary antibodies diluted in DPBS at 4°C overnight. The embryos were then washed for 3 times in DPBS-PVP, and incubated with secondary antibodies diluted in DPBS for 2 hours at room temperature. Then the embryos were washed for 3 times with DPBS-PVP, and then placed in DAPI solution for 15 minutes. Finally, the embryos were washed for 3 times with DPBS-PVP for imaging.

These primary antibodies were used in this study: mouse anti-E-Cad, rabbit anti-Nanog, rabbit anti-Pdgfrα, mouse anti-Yap, rabbit anti-β-cat. Secondary: anti-rabbit 488, anti-mouse 488, anti-rabbit 546, anti-mouse 546. Other antibodies: Nanog 633, F-actin 546, DAPI.

Fluorescent Microbeads Injection

Embryos were placed in 20 μL of KSOM drops covered with 2 mL of mineral oil on a 35 mm

dish. The embryo was held by the holder of the microinjector. We used the needle of the microinjector, which is connected to a syringe to inject fluorescent polystyrene sphere (Thermo scientific) with a diameter of 1 μm into the ICM of the blastocyst.

UV laser cutting

The blastocyst is placed on a glass slide with 20 μL KSOM droplets. After being found under a 40-fold lens field, the center of the blastocyst cavity was penetrated with a UV laser (Power: 30, Aperture: 3, Speed: 13). At the same time, a live cell imaging system was used to record. After the laser cutting is completed, the embryos were quickly transferred to the aforementioned culture environment.

Fluorescence Intensity Analysis

Fluorescence intensity was measured by Fiji ImageJ. We identified every cell in the ICM based on the fluorescence images of DAPI. Through the freehand-selection option, we calculated the average Intensity of Nanog (expressed in nucleus) fluorescence channel. Then the average Intensity of Pdgfrα (expressed on cell membrane) fluorescence channel was obtained by the freehand-line option.

Center of Mass Distance to Lumen Surface

According to images of live embryo expressing $Pdgfr\alpha^{H2B\text{-}GFP/+}$, we connected the geometric center of the ICM and the geometric center of the cavity to obtain the symmetry axis of the embryo. The intersection of the symmetry axis of the embryo and the boundary of the ICM near the cavity was regarded as the center of the ICM. Then we can calculate the distance from the center of cells expressing $Pdgfr\alpha^{H2B\text{-}GFP/+}$ to the center of the ICM.

PIV (Particle Image Velocimetry) Measurement

PIV analysis was performed using a custom algorithm based on MATLAB's PIVlab software package. We use live cell image sequences of embryos to analyze the tissue flow of ICM during

the contraction and expansion of the blastocoel. The average speed is subtracted from calculated velocity fields to avoid the influence of embryo movement on the calculation results. The heat map of ICM's magnitude was also exported after being subtracted the mean velocity.

Shape Index and Cell Tracking

In order to determine the cell boundaries, we used a semi-automatic segmentation pipeline. The cell boundaries of ICM were obtained from the immunofluorescence images of embryos marked with ECA, and then we obtained the perimeter and area. The shape index $i=P/\sqrt{A}$, where P and A are the cell perimeter and projected area. We used the software Bitplane Imaris to get the cell tracking images.

Significant Difference Analysis

Statistical analysis was performed using Excel and R. The continuous quantitative data were analyzed by the normality test first and then compared with the t-test or the Wilcoxon signed-rank test, and $p<0.05$ (two-tailed) was considered as statistically significant.